

This is a post-print of an article that was accepted for publication in Basin Research on January 6th, 2023.

Title:

The evolution of catchment-depositional system relationships on the dip slopes of intra-rift basement highs: an example from the Frøya High, Mid-Norwegian Rifted Margin

Authors:

Gijs A. Henstra*, Aker BP, Oksenøyveien 10, 1366 Lysaker, Norway

Timothy M. Cullen, Department of Earth Science, University of Bergen, PO Box 7800, 5020 Bergen, Norway

Robert L. Gawthorpe, Department of Earth Science, University of Bergen, PO Box 7800, 5020 Bergen, Norway

Jhon M. Munoz-Barrera, Department of Earth Science, University of Bergen, PO Box 7800, 5020 Bergen, Norway

Martin Muravchik, Department of Earth Science, University of Bergen, PO Box 7800, 5020 Bergen, Norway

Atle Rotevatn, Department of Earth Science, University of Bergen, PO Box 7800, 5020 Bergen, Norway

**) corresponding author; gijshenstra@gmail.com*

1 The evolution of catchment-depositional system 2 relationships on the dip slopes of intra-rift basement 3 highs: an example from the Frøya High, Mid- 4 Norwegian Rifted Margin

5 Gijs A. Henstra^{1,2}, Timothy M. Cullen ¹, Robert L. Gawthorpe¹, Jhon M. Munoz-Barrera¹, Martin
6 Muravchik¹, Atle Rotevatn¹.

7 *1. Department of Earth Science, University of Bergen, Bergen, Norway*

8 *2. Aker BP, Oksenøyveien 10, 1366 Lysaker, Norway*

9 **Abstract**

10 Basement highs form one of many potential sediment source areas during the evolution of continental
11 rifts and rifted margins and add to the topographic complexity typical of active rifts. Footwall basement
12 highs acting as a source area to sedimentary systems in the hangingwall of major faults has been
13 documented in many systems worldwide. However, the back-tilted footwall dip slopes of such highs
14 have received comparatively little attention. Here we investigate a subsurface case study from the
15 Norwegian continental shelf, where catchments and shallow marine syn-rift sedimentary systems on a
16 dip slope are preserved due to early transgression of an intra-rift high. At the onset of Late Jurassic
17 rifting, the Frøya High emerged as a prominent, N-S trending, 25 km wide basement high tilted towards
18 the east in response to several kilometers of displacement along the Klakk Fault Complex, a major
19 normal fault zone at the Frøya High's western edge. Using well-calibrated 3D seismic reflection data,
20 we observe a series of conspicuous Upper Jurassic wedges along the eastern edge of the Frøya High
21 along the margin of the Froan Basin. Internally, these wedges show sigmoidal geometries marking top-
22 and foresets of clinoform packages with a maximum thickness of *ca.* 200 meters with foresets between
23 30 – 200 m high, dipping *ca.* 10 degrees towards the east, south east and north east. We interpret these
24 wedges to represent a series of eastward prograding deltas positioned along a constructional shoreline,
25 connected to E-W trending valleys and river catchments updip. The deltas show strong progradation,
26 interpreted to reflect the impact of continued uplift of their catchments. prior to abrupt termination of
27 sediment supply from drainage capture by footwall scarp drainages. The presence of a connected,
28 largely constructional shoreline has implications for Late Jurassic sediment distribution around the
29 Frøya High, providing primary sedimentary input for longshore driven sedimentary systems in the
30 Draugen Ridge to the north. Comparisons with other syn-rift dip slope systems highlights a broadly

31 similar evolution but shows a distinct lack of the protracted backstepping observed in other dip slope
32 systems. We postulate that different structural configurations of dip slope systems, being footwall uplift,
33 or hangingwall subsidence driven, may drive the strongly progradational character of the deltaic
34 systems on the Frøya High. The Frøya High example highlights the need to constrain primary sediment
35 input points to aid interpretation of volumetrically significant, but short-lived and subtle depositional
36 systems, especially within complex, tectonically active settings.

37 **1 Introduction**

38 The evolution of rift basins promotes a wide variety of sediment routing and depositional systems which
39 can vary considerably over relatively short temporal and spatial scales (e.g., Gawthorpe et al., 1994;
40 Ravnås & Steel, 1998; Gawthorpe & Leeder, 2000; Nøttvedt et al., 2000; Barrett et al., 2019). High
41 rates and magnitudes of subsidence in the hangingwall of active structures produce the greatest areas
42 of accommodation, with many studies focussing on the delivery of sediment from drainage catchments
43 on nearby footwall crests (e.g., Bilal et al., 2018; Barrett et al., 2021). However, uplift and rotation of the
44 back-tilted footwall dip slope also offers accommodation for sedimentary systems fed by drainage
45 directed away from the footwall crest. (Ravnås & Steel., 1998; Gawthorpe & Leeder, 2000; Muravchik
46 et al., 2018; Smyrak-Sikora et al., 2018; 2021; Rapozo et al., 2021). The tectono-sedimentary setting
47 of dip slopes developed along the footwall of major faults is considerably different to that of immediate
48 hangingwall systems such as fault-scarp degradation related fans, or rift-margin deltas. Lower gradients
49 and subsidence rates, of backtilted slopes in the footwall of major normal faults, leads to a greatly
50 enhanced sensitivity to eustatic changes across broader, shallower landscapes compared to
51 hangingwall depocentres and commonly host shoreline depositional systems (Gawthorpe et al., 1994;
52 Bell et al., 2018; Fernández-Blanco et al., 2020; Smyrak-Sikora et al., 2021). However, the controls
53 upon the spatial variability in depositional environment and resultant stratigraphic architecture of dip
54 slope shoreline systems in rift settings remains comparatively unclear, especially those flanking large
55 intra-rift basement highs (Nøttvedt et al., 2000; Muravchik et al., 2018). With the exception of few
56 localised outcrop (Jackson et al., 2005; Muravchik et al., 2018; Smyrak-Sikora et al., 2021) and
57 subsurface examples (Ravnås & Steel., 1998; Nøttvedt et al., 2000; Chiarella et al., 2020), there are
58 few studies which address the scales, along-strike variability and potential controls on such syn-rift
59 depositional systems.

60 Offshore Mid-Norway, at the necking domain of the Norwegian rifted margin, the Frøya High hosts a
61 number of fringing syn-rift depositional systems, formed on the footwall dip slope of a major active rift
62 margin bound by the Klakk and Vingleia fault complexes during the Late Jurassic and Early Cretaceous
63 (Figure 1; Blystad et al., 1995; Bell et al., 2014; Elliott et al., 2015; Muñoz-Barrera et al., 2020; Jones
64 et al., 2020). Except for stratigraphy at the northern end of the Frøya High, near the Draugen ridge
65 (Chiarella et al., 2021), syn-rift sediment routing and depositional systems on the eastern flank of the
66 Frøya High have received little attention. The eastern flank of the Frøya High allows for a coherent
67 investigation into the link between sediment source area and down-dip deposition, partly due to partial
68 preservation of drainage catchments on the Frøya High following a prolonged period of flooding and
69 burial of the Frøya High at the end of the Jurassic (Jones et al., 2020). Excellent 3D seismic data

70 coverage and recent exploration drilling in 2022 has allowed for re-evaluation of stratigraphic
71 relationships between the Frøya High and basinal areas with improved constraints through newly
72 acquired biostratigraphic, wireline and sidewall core samples within the Upper Jurassic, Viking Group
73 stratigraphy. Here, we integrate this seismic and well data to investigate syn-rift sedimentation along a
74 footwall dip slope of a major rift-margin normal fault, the Klakk Fault Complex (Figure 1).
75 Biostratigraphically constrained deposits and surfaces permit the mapping and characterisation of
76 three-dimensional variability of syn-rift drainage catchments in the footwall of the Klakk Fault Complex
77 and dip slope the associated dip slope depositional systems at the southern and central part of the Frøya
78 High. Finally, integration and comparison of observations from the Frøya High with other dip slope
79 slope systems from other rift basins demonstrate the variability and role of structural setting in
80 determining the architecture of dip slope sedimentary systems.

81 **2 Geological setting**

82 **2.1 Major tectonic elements and structural evolution of the Frøya High**

83 The Frøya High is situated on the Mid-Norwegian passive margin, between 63°N-64°30'N and 6°30'E-
84 7°20'E (Figure 1) and comprises a granitic basement which delineates a strong positive magnetic and
85 gravity anomaly (Blystad et al., 1995; Olesen et al., 2010; Muñoz-Barrera et al., 2020). It is bounded to
86 the west by the Klakk Fault Complex (KFC) and is located in the necking domain between the
87 hyperextended Møre and Rås Basins (distal domain) and the Trøndelag Platform (proximal domain;
88 Osmundsen and Ebbing, 2008; Mjelde et al., 2009). At the southern part of the Frøya High, the KFC is
89 defined by a 10 – 15 km wide, broad, west-dipping escarpment (Figure 1). The KFC offsets the
90 basement by more than 6 km (Blystad et al., 1995) and reaches the base of the lower crust (Osmundsen
91 & Péron-Pinvidic, 2018; Muñoz-Barrera et al., 2020). The Rås Basin, in the immediate hangingwall of
92 the KFC, has a broadly synformal geometry filled with a ~6-7 km thick Mesozoic-Cenozoic basin fill
93 (Blystad et al., 1995; Muñoz-Barrera et al., 2022).

94 East of the Frøya High lies the southern tip of the 50 km wide Froan Basin that extends for 250 km
95 north along the Trøndelag Platform (Blystad et al., 1995). The Froan Basin is underlain by thick
96 continental crust and contains a Palaeozoic to Cenozoic sedimentary successions. Unlike the western,
97 fault-controlled margin of the Frøya High, the south-eastern margin of the Frøya High passes into the
98 Froan Basin across a gently east-dipping basement-sediment contact cut by several minor, small-
99 displacement normal faults (Figure 1). In the northern part of the Froan Basin this boundary becomes
100 more distinct where the Froan Basin is delimited by a narrow horst between the Vingleia Fault Complex
101 (VFC) and Froan Fault (Figure 1; Wilson et al., 2015; Elliot et al., 2015, 2017; Gernigon et al., 2019;
102 Osmundsen et al., 2021; Bunkholt et al., 2022).

103 The Mid-Norwegian margin evolved through several rift episodes following Devonian collapse of the
104 Caledonian mountain range (Coward et al., 2003; Bell et al., 2014). A major rift episode occurred during
105 the Late Permian – Early Triassic leading to crustal stretching and the formation of NE-SW-trending
106 rotated fault blocks on the mid-Norwegian margin (Brekke & Riis, 1987; Brekke, 2000; Coward et al.,
107 2003; Halland et al., 2013; Péron-Pinvidic et al., 2013;). During this time, a smaller basin was generated
108 on the Frøya High informally known as the Almond Basin, a 2-5 km wide and 0.5 s TWT thick half

109 graben filled largely with, unconfirmed but likely, Permian to Middle Jurassic stratigraphy (Figure 1;
110 Blystad et al., 1995;). Following a period of relative tectonic quiescence from the Mid-Triassic through
111 to the Early Jurassic, extension resumed within the Middle Jurassic through to the Late Jurassic
112 (Færseth, 1996; Brekke, 2000; Coward et al., 2003; Roberts et al., 2009). During this Middle-Late
113 Jurassic phase, the main tectonic elements such as the Møre Basin, the Frøya High and the Halten
114 Terrace started to form as the rift reached a widely documented 'thinning' phase and deformation
115 became localised (Osmundsen et al., 2002; Péron-Pinvidic et al., 2013; Osmundsen & Péron-Pinvidic,
116 2018; Muñoz-Barrera et al., 2020; Bunkholt et al., 2022). The Klakk, Vingleia and Bremmstein fault
117 complexes accumulated substantial displacement at this time and became the location of crustal
118 necking leading to uplift of the Frøya High that emerged as a prominent high, during the latter part of
119 the Middle, and throughout the Late Jurassic – Early Cretaceous within a broader seaway
120 encompassing the approximately 250 km wide and 1500 km long Trøndelag Platform separating
121 Norway and Greenland (Figure 1; Coward et al., 2003; Nøttvedt et al., 2008; Osmundsen & Ebbing,
122 2008; Péron-Pinvidic et al., 2013; Chiarella et al., 2020; Jones et al., 2020; Bunkholt et al., 2022).

123 The Froan Basin itself was only moderately tectonically active during the Late Jurassic – Early
124 Cretaceous rift episode, with a minor component of uplift on its western margin on to the Frøya High in
125 response to uplift in the footwall of the KFC (Blystad et al., 1995). Following the Late Jurassic – Early
126 Cretaceous rift episode, deformation became focused on the distal domain of the Norwegian Margin,
127 west of the Frøya High (Brekke & Riis, 1987; Blystad et al., 1995; Brekke et al., 1999; Osmundsen et
128 al., 2002; Færseth, 2020).

129 Throughout the Early Cretaceous, the crust underneath the Møre Basin became hyperextended with
130 substantial displacement accumulated on the KFC (Grunnaleite & Gabrielsen, 1995; Péron-Pinvidic et
131 al., 2013; Osmundsen et al., 2016; Muñoz-Barrera et al., 2020, 2021; Bunkholt et al., 2022). During this
132 time, uplift of the Frøya High began to decrease and it ultimately became buried during the Mid-Late
133 Cretaceous (Bell et al., 2014; Bunkholt et al., 2022).

134 **2.2 Stratigraphic framework of the Late Jurassic – Early Cretaceous rift episode: the** 135 **Viking Group.**

136 Depositional products of the sedimentary systems that were active on the eastern margin of the Frøya
137 High during the Jurassic – Early Cretaceous rift episode are part of the Middle-Upper Jurassic Viking
138 Group (Figure 2). In the study area the Viking Group either directly overlies the Middle Jurassic Fangst
139 Group, Triassic sediments (known as 'Red' and 'Grey' Beds in local stratigraphic terminology (Blystad
140 et al., 1995), or granitic basement (Figure 2b). The oldest formation of the Viking group is the Callovian-
141 Oxfordian Melke Formation that is commonly interpreted to record the transition from pre-rift to rift
142 initiation in the area of the Frøya High (Blystad et al., 1995; Corfield et al., 2001; Jones et al., 2020;
143 Chiarella et al., 2020). The Melke Formation, where present, is overlain by the Spekk or Rogn
144 formations, that have been linked to 'rift-climax' and late rift phases (Jones et al., 2020). The Spekk
145 Formation is largely mud-prone, high in organic content and is widespread on and around the Frøya
146 High (Jones et al., 2020; Muñoz-Barrera et al., 2020, 2022, Bunkholt et al., 2022;). The Rogn Formation
147 is a distinct sand unit that commonly sits stratigraphically within the Spekk Formation on the eastern

148 flank of the Frøya High (Figure 2b,c, Chiarella et al., 2020). The Rogn Formation is typically interpreted
 149 to represent Late Jurassic – Early Cretaceous deposits of shoreface to offshore-bar environments
 150 (Jones et al., 2020; Chiarella et al., 2020) in a narrow seaway between footwall block islands and the
 151 Late Jurassic coastline of the Norwegian mainland (Chiarella et al., 2020; Bunkholt et al., 2022;
 152 Færseth, 2022). The Viking Group is capped by a regional unconformity, commonly referred to as the
 153 Base Cretaceous Unconformity (BCU) which is overlain by deposits of the mud-prone Lyr and Lange
 154 formations of the Cromer Knoll Group. In most parts of the study area the Cromer Knoll Group onlaps
 155 the BCU. However, the BCU can have a conformable appearance picked out by a high amplitude
 156 negative reflector (Figure 2a).

157 3 Data and Methodology

158 3.1 3.1 Seismic and well data

159 This study makes use of a reprocessed 3D seismic reflection survey that covers most of the southern
 160 part of the Frøya High from the KFC in the west to the Froan Basin in the east (Figure 1a). Seismic data
 161 is in normal polarity, displayed in SEG normal convention (downward increase in acoustic impedance
 162 = positive amplitude). The wells 6306/6-1 and 6306/9-1 provide tie-points for the key seismic markers:
 163 Top basement, Base Viking Group, Top Viking Group (BCU) and base Upper Cretaceous, and Top
 164 Cromer Knoll Group (Figure 2a; Table 1)

165 Well 6306/6-1 is located on the eastern Frøya High and is used to identify the seismic expression of
 166 key stratigraphic events within the syn-rift interval (**Figure 1b, Figure 2**). The sonic and density logs of
 167 well 6306/6-1 provide a record of acoustic impedance contrasts within the stratigraphic interval of
 168 interest and generation of a synthetic seismogram that allows the characteristics of the key stratal
 169 surfaces to be constrained (**Figure 2 and Table 1**).

Well Top Name	Amplitude at 6306/6-1	Character	Variability
Top Basement	High amplitude, hard-kick (positive acoustic impedance).	Moderate lateral continuity.	Occasionally lower amplitude where basement is overlain by Mesozoic stratigraphy.
Base Viking	Zero-crossing from positive to negative from moderate positive amplitude to large negative amplitude.	Moderate-limited lateral continuity.	Amplitude variability common.
Base Rogn Formation	Zero-crossing from negative to positive from weakly negative or noisy wavelet to high positive amplitude.	Moderate lateral continuity.	Laterally consistent.
Top Rogn Formation	Zero-crossing from moderate negative to high positive	Strong lateral continuity	Laterally consistent.

	amplitude often with merged or weakly separated doublet.		
Top Viking Group/'BCU'	Strong-moderate soft-kick to high negative amplitude.	Strong lateral continuity to surface.	Unconformable and laterally variable amplitude character.
Top Cromer Knoll	Zero-crossing to high positive amplitude peak from low-amplitude noisy data.	Strong lateral continuity	Laterally consistent.

170

171 **Table 1: Amplitude characteristics of the key stratigraphic horizons in 6306/6-1 and surfaces**
172 **used in this study.**

173 3.2 Structural restoration

174 Two-way time structure maps (**Figure 3**) generated by detailed manual interpretation of 3D seismic
175 reflection data were depth converted using a velocity model that is based on stacking velocities
176 (Johnson & Hansen, 1987; Marsden, 1989; Ashcroft, 2011) . The accuracy of the resultant depth
177 converted surfaces is independently verified by wells 6306/6-1 and 6306/9-1: the difference between
178 the depth-converted seismic horizons and their actual depth in the wells is less than 20m. We apply a
179 crude structural restoration through a simple 'rigid body' rotation of a depth converted Top Viking Group
180 surface is applied to remove the westward, post-rift tilting associated with continued burial and post-rift
181 thermal subsidence throughout the latter part of the Cenozoic (Brekke, 2000; Bell et al., 2014). This
182 provides an approximation of the topography as it existed during the Late Jurassic. Deformation effects
183 related to compaction and flexure during burial and post-rift thermal subsidence are expected to be
184 minimal and consistent across the study since the area of interest (15 x 20 km) is substantially smaller
185 than the flexure of the Norwegian margin during post-rift subsidence (Brekke, 2000; Bell et al., 2014).

186 4 Seismic mapping

187 The seismic-to-well tie generated for 6306/6-1 (**Figure 2**) is used to characterise the seismic expression
188 of three key stratigraphic contacts: Basement, base Viking Group and top Viking Group/'BCU'. All three
189 reflectors are mapped with high confidence in the eastern part of the seismic reflection survey (**Figure**
190 **3**).

191 4.1 Top Basement TWT structure map

192 The contact between crystalline basement and sedimentary cover corresponds to a positive impedance
193 contrast and a high amplitude, peak (red) reflection where basement is overlain directly by Upper
194 Jurassic/Cretaceous strata (**Table 1, Figure 2**). Where it is overlain by older Mesozoic strata the contact
195 generates a reflection with lower amplitude (**Figure 2, 3**). The seismic expression of the top Basement
196 reflector can therefore be used to help distinguish whether basement is overlain by Upper
197 Jurassic/Cretaceous strata or older Mesozoic strata (**Figure 2, 3**). In the eastern part of the study area
198 the top Basement surface underlies the Late Palaeozoic – Mesozoic infill of the Froan Basin (**Figure**
199 **1c, 4**). There, the contact between basement and sedimentary cover is a non-conformity, relatively

200 smooth, and dips to the east (e.g. **Figure 1c, 4**). In the western part of the study area the basement
201 surface is part of the footwall scarp of the KFC generating the Frøya High (**Figure 3a**). Here, the
202 basement surface dips to the west, is strongly undulating, and is overlapped by Upper Jurassic (Viking
203 Group) and Lower Cretaceous strata (**Figure 1c**). Within the central part of Frøya High the basement
204 surface dips to the east within a half-graben, which is informally known as the 'Almond Basin', and is
205 overlain by pre-Upper Jurassic sedimentary strata.

206 **4.2 Base Viking Group TWT structure map**

207 The base Viking Group surface commonly represents a positive impedance contrast and is expressed
208 mostly as a peak (red) event, but its seismic expression is variable, and it may be expressed as a trough
209 (blue) event locally (Figure 2). This variable expression is related to the unconformable nature of this
210 stratigraphic contact, juxtaposing different lithologies across the contact.

211 The base Viking Group surface is relatively smooth and dips to the northwest across much of the Frøya
212 High and margin of the Froan Basin where the Viking Group overlies the Middle Jurassic conformably.
213 However, with greater proximity to the Frøya High the base Viking Group is increasingly recognised as
214 an angular unconformity (**Figure 1c, 2, 4**). Biostratigraphy from 6306/6-1 and 6306/9-1 records a
215 hiatus across this surface that may span the Bajocian (Statoil, 1994). In areas along the southern part
216 of the Frøya High, and underlying a N-S oriented concave-up trench on the western edge of the Froan
217 Basin, the Base Cretaceous Unconformity ('BCU') has eroded down to the pre-Upper Jurassic interval.
218 As a result, the Base Viking Group surface is coincident with the Top Basement surface where Middle
219 Jurassic stratigraphy is absent ("deeply eroded" areas on **Figure 3b**).

220 The distribution of the Viking Group is more complex on the Frøya High than in the Froan Basin. Where
221 the Viking Group is preserved it may rest either on crystalline basement, or on Lower Mesozoic
222 stratigraphy (e.g. **Figure 4**). The latter form is most common, especially overlying the Almond Basin
223 where the greatest areal extent of Viking Group stratigraphy is preserved on the Frøya High (**Figure 5**).
224 Where the Viking Group overlies the Permian and Middle Jurassic of the Almond Basin, the Base Viking
225 Group surface is an angular unconformity of around 15 degrees with older stratigraphy within the
226 Almond Basin (**Figure 4**). Upper Jurassic, Viking Group stratigraphy noticeably overlies relative palaeo-
227 highs on the central and western part of the Frøya High as well as three small (1 – 2.5 km wide) highs
228 on the eastern part of the Frøya High on the flank of the Froan Basin (**Figure 3b**)

229 **4.3 Top Viking Group (BCU) TWT structure map**

230 The top Viking Group/'BCU' surface marks a negative impedance contrast and corresponds to a trough
231 (blue) event at the intersection with 6306/6-1. However, its amplitude changes spatially recording the
232 variable lithology of underlying and overlying stratigraphy (**Figure 2**). It represents an erosional surface
233 that is generally broadly parallel to the underlying strata across much of the Frøya High and margin of
234 the Froan Basin, but locally is a down-cutting surface, eroding deeply into the substrate, that has a
235 concave-up geometry with relief of 50-200 m in parts of the southern Frøya High and within the Froan
236 Basin (X on **Figure 3c, 4**). Overall, the surface deepens to the west with localised regions of steepening
237 gradient along the eastern edge of the Almond Basin, and along a N-S running ridge 2 – 3 km west of

238 the western edge of the Almond Basin (D on **Figure 3c**). There are several regions of onlap onto relative
239 palaeo-highs, typically 1-5 km in diameter and ~40-50 m high on the eastern side of the Frøya High,
240 and a small cone shaped, 2 km wide region west of the Almond Basin across an area of steepening
241 gradient of the BCU (**Figure 3c**).

242 **4.4 The Viking Group isopach map**

243 The Viking Group isopach map reveals substantial spatial variability in thickness (**Figure 3a**) with a
244 relatively large, 20 km wide, depocentre overlying, and east of the previous Almond Basin (Depocentre
245 O; **Figure 5a**), with ca. 150 m of Viking Group stratigraphy. In the southern part of the Almond Basin
246 these strata are truncated and deeply eroded by the BCU forming a ~15 km long, 10 km wide depression
247 that cuts down progressively deeper towards the south-west reducing the thickness of the Viking Group
248 to <10 m and locally making it absent (**Figure 3b,3c, 4, 5a**). A few kilometers to the east of the Almond
249 Basin are three accumulations of Viking Group strata up to 300 - 250 m thick each measuring ca. 5 km
250 in width (Depocentres A, B and C; **Figure 5a**). These accumulations show approximately fan-like
251 geometries in plan view, with radial thinning from their centres and are separated by narrow (1-3 km)
252 wide regions of zero or very limited thickness (Areas I, II, and III **Figure 5a**). Immediately east of these
253 wedges angular truncations of Upper Jurassic (Viking Group) and Middle Jurassic stratigraphy and a
254 substantial decrease in Viking Group thickness suggest widespread erosion along a N-S trending
255 depression (Figure 4b, Figure 5). The N-S depression (Area E; Figure 4b) has a jagged western edge,
256 approximately 25 km long and 3-5 km wide with a maximum relative depth of ~500 m (Area E; **Figure**
257 **5b**). Farther to the north-east, closer to the centre of the Froan Basin, the Viking Group is preserved
258 and exhibits a relatively uniform thickness between 30 – 40 m over a 5 x 5 km area (Depocentre D;
259 **Figure 5a**). Overall, the variable thickness patterns are interpreted to represent both non-uniform
260 deposition in Jurassic times and subsequent erosion during the Early Cretaceous.

261 **4.5 The Cromer Knoll Group isopach map**

262 The top of the Viking Group, commonly referred to as the BCU, marks the base of the Cromer Knoll
263 Group isopach. The BCU is marked by onlap by the lowest part of the Cromer Knoll Group in parts of
264 the crestal areas of the Frøya High (e.g., D in Figure 4c) and is conformable within areas on the eastern
265 margin of the Frøya High and in the Froan Basin (e.g. F in Figure 4). The Cromer Knoll Group is
266 relatively thin (25 m or less) or absent over the crestal and eastern part of the Frøya High (Area A,
267 Figure 4). . Conversely, in the Froan Basin to the east there are substantially thicker accumulations of
268 Cromer Knoll Group stratigraphy (Area E and F, **Figure 4, 5b**). The large, N-S trending erosional feature
269 hosts up to 500 m of Cromer Knoll stratigraphy which onlaps the BCU within Area E, becoming generally
270 thicker towards the south of and east of the feature (**Figure 4, 5b**). To the northeast within the Froan
271 Basin, thicknesses of up to 300 m of Cromer Knoll group are observed (**Area F on Figure 5b**).

272 This spatial pattern of thickness of the Cromer Knoll Group and onlap is interpreted to reflect the
273 progressive flooding of the Frøya High, with the Frøya-Froan margin and the crestal part of the Frøya
274 High being one of the last areas to be flooded during the early Cretaceous (Brekke et al., 2000; Bell et
275 al., 2014; Jones et al., 2020). Unlike the Viking Group isopach map, the lateral variability in thickness
276 of this interval is attributed mostly to non-uniform deposition on a variable underlying topography with

277 the majority of the Lower Cretaceous deposits of the Cromer Knoll Group being non-erosional and
278 internally conformable for the most part. The Froan Basin in the easternmost part of the study area
279 continued to receive sediment since earliest Cretaceous times (Depocentre F; **Figure. 5b**; Skarbø et
280 al., 1988). The large, N-S-trending erosional feature is interpreted to have been excavated during the
281 early stages of the Early Cretaceous by the removal of Upper Jurassic and older strata had become
282 filled by the end of the Early Cretaceous as evidenced by onlap of Cromer Knoll reflections onto the
283 BCU on either side of the erosional depression (Depocentre E; **Figures. 5b, 4**).

284 **5 Seismic and wellbore stratigraphy and geomorphological characterization of the Viking** 285 **Group on and around the Frøya High**

286 Observations

287 The seismic stratigraphic architecture within the Viking Group fan-shaped, wedges (A, B and C; Figure
288 5a) is relatively complex in comparison to the expression of the Viking Group elsewhere (Figure 6). By
289 flattening the seismic on the Top Cretaceous horizon (Top Shetland Group) we can approximately
290 restore the orientation of the reflectors that make up the wedge to their original geometry before the
291 area became tilted towards the west (Figure 7). On the flattened data, the western and upper part of
292 the wedges consists of parallel, horizontal to sub-horizontal reflections that onlap the basement/base
293 Viking Group surface to the west. To the east, the wedges consist of east-dipping, inclined, sigmoidal
294 reflections that downlap the basement/base Viking Group (**Figure. 4, 6, 7**). The maximum (non-
295 decompacted) thickness of the wedges amounts to ~250meters (**Figure. 4, 7a**) and the internal
296 sigmoidal reflectors dip ca. 10 degrees. Heights of inclined reflectors vary from ~30 – 200 m. When
297 viewed in aNE-SW section u, reflections have apparent dips in opposing directions, away from the
298 approximate centre of each wedge and generate broadly convex-up internal morphology with internal
299 complexity and surfaces marked by downlaps (**Figure 8**).

300 Well 6306/9-1 penetrates Wedge B and recovers approximately 155 m of Middle to Upper Jurassic
301 which lies directly on crystalline basement (**Figure 9**). Biostratigraphic and sedimentological analysis of
302 sidewall cores are integrated with wireline and borehole image data into a summary log in Figure 9. The
303 Middle Jurassic stratigraphy comprises a sub-horizontally bedded basal section following bed
304 restoration, from ~941-967 m depth, of interbedded fine-medium-grained sandstone and siltstone rich
305 in carbonaceous material and root traces, which is capped by a coarser grained, upward fining gravelly
306 sandstone rich in carbonaceous material but also calcareous shell fragments (**Figure 9**). Palynological
307 observations in this section show substantial presence of brackish water indicators typical of a marginal
308 marine assemblage and is dated as Callovian. The basal section transitions abruptly at ~940 m depth
309 into a clay-rich, non-bioturbated siltstone with low palynological diversity at the onset of a largely silt
310 and clay-prone, ~45 m thick Oxfordian section becoming increasingly bioturbated and sand-prone
311 upwards (**Figure 9**). This is overlain by an abrupt transition at 895 m into sand-prone sidewall core
312 samples and consistently low gamma-ray values with a marked reversal in neutron-density separation
313 (**Figure 9**). This section is dated as Kimmeridgian-Volgian with extensive reworking of Oxfordian
314 palynomorphs and coincides with the position of well recognised eastward dipping, downlapping
315 reflections in the seismic data (**Figure 6**). In the well, this is recognised as a change of restored bedding

316 dips to steeper (c. 25°), exclusively eastward dips. The Kimmeridgian section can be split into three
317 subunits (**Figure 9**) comprising medium-very coarse sandstone-prone packages separated by the
318 shallower dipping (c. 10°) 1-2 m thick argillaceous sandstone beds. The three sub-units broadly
319 demonstrate a steepening to shallowing restored bedding trend punctuated by shallower restored
320 bedding within the intervening argillaceous sandstone intervals (**Figure 9**). Sandstone beds are typically
321 coarse-grained, granule-bearing and poorly sorted, with occasional development of cross-stratification
322 and abundant organic material. The section returns at 847 m depth to dominantly fine-to medium-
323 grained sandstone that is still granule-bearing and displays planar to cross-stratification coincident with
324 a move into shallowly eastward dipping, planar reflectors in seismic section (**Figures 6, 9**). However,
325 this package ultimately becomes Ryazanian aged and increasingly rich in glauconite pellets and is more
326 intensely bioturbated (*Chondrites* and *Palaeophycus*). This is capped at 819 m depth by a relatively
327 thin, 7 m section of intensely bioturbated, coarse to very coarse, sub-horizontally bedded sandstone
328 (**Figure 9**). The sandstone itself is overlain by gravel- and pebble-rich sandstones (813 – 815 m) with
329 broken shell fragments and heavy minerals that account for extremely high gamma readings (**Figure**
330 **9**). This is overlain by a sub-horizontally bedded claystone with pervasive *Chondrites* at 812 m depth,
331 coinciding with the position of the strong negative amplitude associated with the Top of the Viking Group
332 in seismic (**Figures 6, 9**)

333 The Top Viking Group/BCU structure map and isopach maps show that the eastern edge of the wedges
334 has an irregular, jagged, erosional, appearance in plan view marking the edge of the N-S erosional
335 feature highlighted by the base of Depocentre E (X in **Figure 3c, 10**). The N-S erosional feature has
336 connection along its western edge to 0.5 – 1.5 km wide, smaller scale erosional features trending NW-
337 SE or E-W, which shallow to the west onto the Frøya High. The irregular nature of the BCU at the
338 eastern edge of the wedges also hosts numerous, relatively small (ca. 100 m wide and 500 m long),
339 amphitheatre-shaped depressions that shallow westwards (**Figure 10**). Isopach maps reveal that the
340 Viking Group is thinner within these features (**Figure 5a, 10**) and that they are filled in with, younger,
341 Cromer Knoll stratigraphy, that onlaps this surface (**Figure 5b, 10b**).

342 Interpretations

343 We interpret the Viking Group wedges with their internal sigmoidal reflections as clinoforms. Based on
344 their fan-shaped plan view geometry of the three wedges (A, B, and C and D; **Figure 5a, 7**) and eastward
345 dipping and prograding foresets, the wedges are interpreted as eastward prograding deltaic packages.
346 Observations of carbonaceous, rooted heterolithic sandstones from 6306/9-1 suggest the deltaic
347 clinoforms are preceded by a Callovian-aged coastal plain containing occasional fluvial channels which
348 became transgressed in the Oxfordian establishing a largely dysoxic, mud-prone shelf and increasingly
349 sand-prone prograding shoreface rich in bioturbation. This backstepping is followed by the strongly
350 progradational deltaic clinoforms observed on seismic (**Figure 6, 7b**) which are seen to be that of a
351 coarse-grained sand-prone and poorly sorted, eastward prograding delta initiated during the
352 Kimmeridgian (**Figure 9**). The observed height and relatively steep (>10°) angle of the clinoform
353 foresets indicates progradation into a waterbody up to ~200 m deep towards the upper, later part of the
354 Viking Group section. Smaller foresets (from 30-50 m) during the onset of the clinoform packages

355 (Figure 6) indicate periods of less accommodation early in the history of the deltas increasing in height
356 through younger clinoforms, with foreset height through the deltas depending on the interaction of sea-
357 level and seafloor topography at a given time (**Figure 7, 9**). Argillaceous sandstones intersected in the
358 wells demonstrate similar thicknesses and characteristics to reactivation surfaces separating foreset
359 packages documented in fan deltas (e.g., Backert et al., 2010; Gawthorpe et al., 2017; Barrett et al.,
360 2019). Similarly, the scales (10-30 metres thick) and lithology (coarse-grained, gravel-pebble prone
361 sandstones) of the steeper cross-stratified sub-units are comparable to that of Gilbert-type fan deltas
362 with steeply dipping delta fronts comprising a broad range of gravity flow deposits (Massari & Collela,
363 1988; Nemeč, 1990; Rohais et al., 2008; Gobo et al., 2014; Barrett et al., 2019; Chiarella et al., 2020).

364 The arcuate, amphitheatre-shape of some of the erosional features (**Figure 5, 10**) resemble the scars
365 left by slumping of unconsolidated material observed on modern subaqueous depositional slopes (e.g.,
366 Biscara et al., 2012; Gales et al., 2019) and in outcrop (Postma 1984; Backert et al., 2010; Gobo et al.,
367 2014; Rubi et al., 2018). Similarly, they could also represent longer lived tributaries into the larger N-S
368 directed erosional features. The current dataset is not sufficient to conclude whether the N-S-trending
369 erosional feature (Area E; **Figure. 4, 5b, 5**) formed concomitant with the clinoform package or if it is a
370 younger and distinct, separate feature. However, the main erosional surface of the BCU is locally
371 underlain by slightly older, intra-Late Jurassic erosive features within the northern most part of
372 Depocentre E (Figure 5b, 7d) suggesting that the head of this feature may have initiated during the Late
373 Jurassic, with minor periods of filling, prior increased erosion as part of a larger, subaqueous drainage
374 system during the Cretaceous.

375 **6 Structural restoration of the Late Jurassic rift terrain**

376 The Upper Jurassic clinoform packages on the Frøya High, particularly their topsets that were deposited
377 in a near-horizontal coastal plain or shallow marine platform setting, may provide constraints on the
378 amount of tilting that has occurred since Late Jurassic times.

379 **Figure 11** shows the depth-converted section rotated by 20 degrees on the basis the western flanks of
380 the clinoform packages are interpreted to be sub-horizontal topsets during the Late Jurassic. The
381 resultant section (**Figure 11c**) represents an approximation of the attitude of sedimentary rocks of the
382 Viking Group on the Frøya High at the time of deposition (Figure 12). Our simple approach does not
383 incorporate flexure and compaction and is less accurate away from the anchor point, Viking Group
384 wedge 'B' on **Figure 5a**, and especially where uplift would be greater, closer to the KFC. Additionally,
385 the Top Viking Group/BCU structure map is a composite surface which in places is conformable (e.g.,
386 near 6306/6-1 and 6306/9-1), but in others reflects substantial erosion (e.g., areas marked '1', '2' and
387 '3' on **Figure 12**). In areas where the Viking Group was partially removed during the post-rift phase the
388 surface contains topographic elements that post-date the Jurassic and so may not reflect the Late
389 Jurassic configuration of the surface within those specific areas. Despite these shortcomings of our
390 simple approach, the restoration of **Figure 11, 12** performs well in the eastern flank of the Frøya High
391 and within the clinoform packages where there is limited post-Late Jurassic erosion. The restoration
392 suggests that a prominent irregularity on the basement contact immediately west of the Almond Basin
393 ('y' in **Figure. 11b**) formed a topographic high during late Jurassic times (**Figure 11c**). The thickness

394 maps of **Figure 5** reveal that this topographic high corresponds to an area of non-deposition during the
395 Late Jurassic (**Figure 5a**) and to some extent also during the Early Cretaceous (**Figure 5b**). Together,
396 these observations suggest that this north-south trending basement ridge likely represented the apex
397 of the Frøya High during the Late Jurassic seen in both the Viking Group thickness map and the restored
398 Top Viking Group structure map (**Figures 5a and 12**). We interpret this ridge to represent the drainage
399 divide of the Frøya High as it existed during Late Jurassic- and possibly Early Cretaceous times (**Figure**
400 **3**).

401 **7 Late Jurassic palaeo-drainage and palaeogeography of the Frøya High**

402 The interpreted prograding shoreline-delta system developed east of, and parallel to, the eastern margin
403 of the Almond Basin. The structural restoration of **Figure 12** suggests that the Almond basin was
404 positioned topographically higher than the clinoform packages during Late Jurassic times and was likely
405 subaerially exposed when the clinoform packages were prograding. In addition, the interpreted palaeo-
406 drainage divide of the Late Jurassic was located parallel to and immediately west of the Almond Basin.
407 These interpretations together allow constraint on the position and geometry of the palaeo-catchments
408 which fed the clinoform packages, and broadly encompass the area 'O' in the Upper Jurassic thickness
409 map of **Figure 5a**.

410 Each of the distinct Upper Jurassic clinoform packages (A, B, C in **Figure 5a, 13**), are connected to to
411 the central portion of the Frøya High (Area O – Figure 5a) through three, substantially thinner, but
412 narrow corridors of Upper Jurassic deposits (**Figure 5a**). Each of these narrow corridors are separated
413 by areas where the Upper Jurassic stratigraphy is extremely thin (<20 m) or largely absent (I, II and III
414 on **Figure 5a**). In these areas (I, II and II on Figure 5a) the strong negative acoustic impedance, linked
415 to organic rich shales typical of the Top Viking Group is still preserved (e.g., intersection with Area II in
416 **Figure 7b**), and so indicates these areas do not simply represent enhanced Early Cretaceous erosion
417 unlike deeply eroded areas of Viking Group stratigraphy. We interpret the thickness patterns of the
418 Viking Group to reflect that the geometry of palaeo-catchment area 'O' (**Figure 5a**) was likely subdivided
419 into a series of parallel drainage catchments with SE-flowing river systems that debouched to the
420 southeast and supplied sediment to individual point-sourced fan deltas between areas I, II and III
421 (**Figures 5a and 13**). The area occupied by the palaeo-catchment on the restored structure map of
422 **Figure 12** is affected by Early Cretaceous erosion, which renders it inadequate for mapping more subtle
423 features of Late Jurassic such as individual drainage profiles. However, the restoration does provide
424 some constraints on overall catchment geometries.

425 Measuring from the maximum eastern (basinward) extent of the Viking Group thickness anomalies to
426 the interpreted drainage divide provides an approximate maximum catchment length of 12.5 km, 16.9
427 km and 18.3 km for clinoform package A, B and C respectively with a mean catchment length of 15.9
428 km (Supplementary Information). The catchment for clinoform package D is only partly covered by the
429 dataset and so the length is difficult to constrain. The total basinward extent of the Viking Group
430 thickness anomaly probably overestimates the catchment length as it includes a portion of subaerial
431 topset, subaqueous foreset and bottomset which is not part of the subaerial catchment (Hovius, 1996).
432 Alternatively, the location of catchment outlets can be estimated from the isopach map as the region

433 where there is an abrupt widening and onset of a fan-like geometry of the thickness anomalies. Using
434 the estimation of the catchment outlet provides a minimum estimate of the catchment length which are
435 8.0, 11.3, and 12.1 km for clinoform package A, B and C respectively, giving an average length of 10.5
436 km, and indicating an average clinoform package length of 5.2 km (Supplementary Information). These
437 dimensions are in keeping with ancient and modern deltaic clinoforms observed in the Corinth Rift (e.g.,
438 Barrett et al., 2019), and measurements in compiled database studies for sand-prone deltaic clinoforms
439 (Patruno et al., 2015).

440 The spacing between catchments can be roughly estimated using the small, 1-5 km long, ~100 m
441 high, relative highs (I, II and III on **Figure 5a** and **Figure 13a**) and assuming that the catchment outlets
442 were located centrally between them. This analysis gives catchment spacings of 5.7 km between C and
443 B, and 7.6 km between B and A, averaging 6.7 km, or 6.3 km if the Viking Group thickness anomaly
444 (Wedge D) north of Wedge A, to the west of 6306/6-1 is also included (Supplementary Information).
445 The spacing ratio of catchment length to spacing averages 1.69 using minimum length estimates, and
446 2.4 using maximum length estimates, in keeping with catchment area morphometrics for active basins
447 in other studies (2.07 – Hovius, 1996; 2.5 – Talling et al., 1997; 2.48 Sømme et al., 2010). The area of
448 the catchments ranges between 44 – 104 km², which is typical for small catchments common in active
449 rift margins (e.g., Eliet & Gawthorpe, 1995).

450 Characterisation of the Frøya High bedrock stratigraphy highlights that Late Jurassic catchments
451 consisted of relatively easily erodible sedimentary rocks of Upper Palaeozoic – Lower Mesozoic age
452 within the Almond Basin, as opposed to the crystalline rocks elsewhere, outside the Almond Basin, on
453 the southern Frøya High (Jones et al., 2020; Munoz-Barrera et al., 2020, 2021). We conclude on the
454 basis of spatial patterns of Viking Group thickness, the position of a NE-SW trending ridge following
455 restoration, and comparison with other rift system catchment morphometrics, that the interpreted Upper
456 Jurassic clastic shoreline system was supplied by at least four distinct drainage basins, each around
457 ~10 km, long spaced 5.5 – 7.5 km along the dip slope of the Frøya High. Each drainage basin was
458 preferentially located on exposed pre-Middle Jurassic sedimentary rocks of the Almond Basin which
459 provided easily erodible material feed clinoform packages that prograded eastward into the Froan
460 Basin.

461 **8 Early Cretaceous evolution of the Frøya High**

462 The erosional features of the Top Viking Group/BCU surface removed substantial portions of the Upper
463 Jurassic stratigraphy (e.g. Area 1 – 5 on **Figure 12**, **Figure 13b**). The timing of this erosion is poorly
464 constrained and it is possible that it could have commenced during the end of the latest Jurassic (e.g.
465 sub-BCU erosive features on **Figure 7d**) .. Areas 1 – 3 exhibit a broadly N-S-orientation, compared to
466 E-W orientation of the Late Jurassic drainage catchments (**Figure 12** **Figure 13**). Moreover, these areas
467 seem to represent catchments that drain towards the southwestern edge of the Frøya High. Areas 4
468 and 5, however, have the same location and orientation as their corresponding Late Jurassic erosional
469 features (Figure 12, 13). It thus follows that those catchments that drained westward into the Møre
470 Basin were not rearranged during the transition from the Late Jurassic to the Early Cretaceous. Those
471 Jurassic catchments (Areas 1 – 3) that used to be contained within the east-facing dip slopedip slope,

472 however, underwent significant change. A clear indication of the mechanism behind this rearrangement
473 of drainage on the dip slopedip slope is suggested by Area 3 (**Figure 13b**), where headward erosion
474 from one of the fault scarp-bounded catchments (**3 on Figure 12 and 13b**) appears to have captured
475 a large portion of the catchment that was previously draining eastward. The final form of the erosive
476 features (e.g., 1-5 on **Figure 13b**) is interpreted to be of Early Cretaceous age as large portions of
477 Upper Jurassic stratigraphy that covered the Almond Basin, likely deposited during transgression of the
478 Jurassic drainage basin ('O' in **Figure 5**), were eroded by the younger, southward draining catchment.
479 We propose that this must have occurred as the footwall scarp catchments along the KFC continued to
480 grow by headward erosion.

481 Although the relatively deep, southward directed canyon immediately east of the clinoform package
482 (Area 2, in **Figure 12**) extends south beyond the study area it seems plausible to be the result of a
483 similar drainage capture event that could have occurred farther to the southeast along the KFC fault
484 scarp. Observations of degradation of the delta foresets, and of sub-BCU erosion in the northern part
485 of this erosive feature (e.g., Figure 7d) indicate that the Area 2 canyon may have begun forming whilst
486 the clinoform packages were active during the Latest Jurassic. Here, degradation of the clinoform delta-
487 front may have facilitated sediment transport into and along the basin floor in an axial channel system
488 not dissimilar to axial channels observed in front of modern fan deltas (e.g. Prior & Bornhold, 1989;
489 McNeill et al., 2005; Beckers et al., 2018; Gales et al., 2019; Gawthorpe et al., 2018). However, the
490 data is not able to resolve how much of this erosion substantially post-dates the emplacement of the
491 clinoform packages (i.e during the Early Cretaceous), and is formed by more widespread, headward,
492 subaqueous erosion of the then submerged Frøya High flank. Nevertheless, the isolated positions of
493 Cromer Knoll Group thicknesses and onlap of the Cromer Knoll Group onto the BCU suggest that the
494 topography of Area 2 within the canyon was in place by the end of the Early Cretaceous (**Figure 4, 7,**
495 **13**).

496 The canyon at Area 2 likely formed a substantial topographic/bathymetric low within which the Cromer
497 Knoll Group was deposited (**Figure 13**) and may well have formed through a composite history of both
498 Late Jurassic and Early Cretaceous erosion. The Lower Cretaceous Cromer Knoll Group in the study
499 area consist of continuous, sub-parallel strata that onlaps the BCU with some minor concave-up
500 geometries within the broad N-S orientated erosional feature (Area E, **Figure 4, 6, 7d**). The lack of any
501 major constructional features along the flank of the Frøya High (cf. Upper Jurassic clinoform packages)
502 suggests that the Frøya High depositional systems which routed sediment towards the Froan Basin
503 likely shutdown and that sediment routing was largely focussed to the south and west of the Frøya High
504 through the Early Cretaceous. A termination of sediment supply from region O (**Figure 5**) is in
505 agreement with the gradual onlap of the Frøya High by the Cromer Knoll Group, recording a relatively
506 fast transgression of the Frøya high at the end of the Jurassic and into the Early Cretaceous (**Figure**
507 **3c; 9**; Brekke, 2000; Bell et al., 2014; Jones et al., 2020).

508 **9 Discussion**

509 **9.1 Alternative interpretations of the studied clinoform packages: The Rogn** 510 **Formation as a connected, constructional coastline on the Frøya High**

511 Our interpretation of the Upper Jurassic packages on the southeastern part of the Frøya High as deltaic
512 clinoform packages is different from earlier interpretations. Chiarella et al. (2020) propose the same
513 sand-prone packages within the Rogn Formation to be interpreted as coastal sand ridges sourced and
514 constructed solely through longshore currents, using comparisons between core from the well 6306/6-
515 1 and the Draugen field 100-125 km to the north-east (also described by Van der Zwaan, 1990). Deltaic
516 clinoforms are our preferred interpretation on account of the lobate, convex to the east plan view
517 geometry, eastward progradation, consistent with an overall upward coarsening, poorly sorted, coarse-
518 grained foreset-dominated package in 6306/9-1 (**Figure 9**), typical of fan deltas (e.g., Nemeč 1990;
519 Rohais et al., 2008). Furthermore, the location of the clinoform packages down-dip of a prominent,
520 erosional, drainage catchment-liked geometries, floored by highly erodible sedimentary deposits of the
521 Almond Basin implies the bulk of sediment was deposited within deltas at the coastline with only minor
522 reworking and northward transport of sediment within delta topset deposits (e.g., Figure 9, Figure 13,
523 14). The clinoform packages all exhibit a consistent progradational architecture from west to east, with
524 parallel topsets overlying or connected to generally east-dipping sigmoidal clinoforms when Upper
525 Mesozoic and Cenozoic rotation is removed by flattening onto a Top Shetland Group horizon (**Figure**
526 **7**). Chiarella et al. (2020) do refer to westward dipping foresets in the northernmost part of the dataset,
527 immediately west of 6306/6-1. However, we observe only a single westward dipping surface (**Figure**
528 **7d**) which ties downdip into the large N-S trending erosional feature (e.g. Depocentre E, **Figure 5**). We
529 therefore interpret this westward dipping reflector to be the margin of the up-dip head of this erosional
530 feature that post-dates the delta itself. The consistent eastward progradation is more compatible with
531 that of a radial fan delta than with an offshore sand-ridge, which would likely show coastline parallel
532 progradation. Whilst progradational clinoforms do form within offshore sand ridges (e.g., Berne et al.,
533 1998) their angle is typically less than 10 degrees, and foreset heights rarely exceed 30 meters
534 (Chiarella et al., 2020), an order of magnitude smaller than the maximum height of those observed in
535 the Frøya High study area. The abundance of bioturbated, macro-fossiliferous, plant material-rich facies
536 of the Rogn Formation described in 6306/6-1 by Chiarella et al. (2020) and used to ascribe a sand-ridge
537 interpretation are not necessarily unique to that depositional environment. Bioturbation, macro-fossil
538 and plant-material rich sandstones are common in a broad range of shoreline and near-shoreline
539 depositional environments and are especially common in wave- or tide-modified delta fronts (Gustaldo
540 & Huc, 1992; Rossi & Steel, 2015; Anell et al., 2020)..

541 Our interpretation of the studied Upper Jurassic clinoform packages as a series of fan deltas has
542 implications for the overall depositional setting and sediment flux across the eastern flank of the Frøya
543 High during the Late Jurassic. **Figures 13 and 14** illustrate a new, depositional model that shows a
544 coastline along the eastern side of the Frøya High that is more constructive and dominated by
545 transverse sediment input, rather than axial reworking that has dominated previous models driven by
546 observations from the Draugen sand ridge (e.g. Van der Zwaan, 1989; Chiarella et al., 2020).
547 Palaeocurrent measurements from 6306/9-1 do suggest a component of longshore reworking near the
548 top of the Rogn Formation, however we interpret this to be limited to reworking within the topsets of
549 deltas, with the large thicknesses of sediment within the proposed deltas suggesting considerable
550 volumes of sediment are stored within the deltas rather than transported further northwards.

551 Whilst the existence of shallow marine systems flanking the transition between the Frøya High and
552 Froan Basin have long been speculated on the basis of observations from the Draugen Field (Van der
553 Zwaan, 1989; Chiarella et al., 2020), we speculate further that the Draugen sand ridge may be more
554 intimately related to the regressive, deltaic shoreline documented here. Existing interpretations for
555 sedimentation of the Draugen Ridge lacked a demonstrable sedimentary input for sediment reworked
556 axially from the southwest. The proto-Norwegian Sea existed as a narrow seaway located above 30
557 degrees latitude from the early through to the Late Jurassic. Palaeoclimate interpretations for the Late
558 Jurassic and Early Cretaceous of the North Sea and NW Europe (e.g. Abbink et al., 2001; Mutterlose
559 et al., 2003) highlight that the prevailing current direction was controlled by the northern hemisphere
560 westerlies, i.e. directed to the north east. These current directions are consistent with the dune migration
561 direction proposed in Chiarella et al. (2020) for the asymmetry of the Kimmeridgian Rogn Formation at
562 the Draugen field, and with Early Jurassic Ilje Formation shallow-marine bar progradation, and long-
563 shore sediment redistribution in the Halten Terrace (Martinius et al., 2001). As a result of these
564 westerlies, the northwestern margin of the Frøya High likely received a strong northeastern current as
565 the southern part of the Sklinna Ridge was submerged and formed an opening to the proto-Norwegian
566 Sea to the west (Bell et al., 2014; Elliott et al., 2015, 2017). Similar currents along the eastern flank of
567 the Frøya High were also likely in operation due to the same prevailing current direction, which may
568 have been enhanced through interaction of the several exposed islands in the narrow seaway of the
569 proto-Norwegian sea (**Figure 14**). Petrographic information of the Kimmeridgian Rogn Formation at the
570 Draugen ridge (Van der Zwaan, 1990; Chiarella et al., 2020) and broader Møre-Trøndelag area (Mørk
571 & Johnsen, 2005) indicate a provenance with minor reworking from local granitic and Mesozoic-
572 sediment covered palaeohighs such as the Frøya High to the south and west of the Draugen Ridge and
573 Froan Basin (Jongpier et al., 1996; Mørk & Johnsen, 2005). This petrographic signature is consistent
574 with a redistribution of sediment along strike in the shoreline region of the Frøya High – Froan basin
575 margin, with the confluence of these currents meeting at the Draugen Ridge, on the eastern tip of the
576 Vingleia Fault (**Figure 14**). The deltaic clinoform systems recognised in this study in the southern part
577 of the Frøya High likely provide the primary sedimentary input for the more minor amount of sediment
578 which may be reworked along the Frøya High-Froan basin margin. The description of the Draugen ridge
579 presented by Van der Zwaan (1989) and Chiarella et al. (2020) along with our model of redistribution is
580 consistent with the prediction by Nielsen & Johannessen (2009) of how spit systems will often locate at
581 the confluence of meteorological oceanic currents around a landmass, along-strike from major sediment
582 input points, where a majority of sediment remains. The stratigraphic architecture recognised in
583 Chiarella et al. (2020), with a large subaqueous, mud-dominated platform on which upward-coarsening
584 units from a subaerial, high-energy environments are deposited also bear similarities with modern and
585 recent spit environments documented in Nielsen & Johannessen (2009).

586 **9.2 Implications for models of clastic shoreline sedimentation on rift-related dip** 587 **slopedip slopes**

588 **9.2.1 Impact of hinterland characteristics and source-to-sink configuration on depositional** 589 **systems around intra-basinal highs**

590

591 In the case of the Frøya High, the nature of the bounding structures and resultant physiography of the
592 Late Jurassic landscape can produce substantial along strike variability in the nature of the coastline.
593 This case study demonstrates that if a relatively sizeable source for sediment is exhumed during the
594 evolution of a rift, even in an intra-basinal location, constructive coastal environments may develop
595 locally on dip slopedip slopes, especially downslope of easily erodible sedimentary bedrock. At the
596 southern edge of the Frøya High, a relatively broad, backtilted, footwall dip slope consisted of an easily
597 erodible exhumed sedimentary basin (the Almond Basin) that supplied sediment to a series of closely
598 spaced fan deltas and resulted in a regressive coastline. Less than 100 km to the north, where the
599 Frøya high is significantly narrower and consists of resistant, crystalline bedrock, sediment supply is
600 likely dependent on longshore drift (Van der Zwaan, 1989; Chiarella et al., 2020). The longshore drift
601 dominated coastlines in this region may be dominantly transgressive compared to more progradational
602 or aggradational time-equivalent systems along-strike to the southwest. Muravchik et al. (2018)
603 highlight the co-existence of sediment starved dip slopeand delta-fed dip slopes over strike distances
604 of 10-20 km-from the El-Qaa fault block of the Suez Rift. Muravchik et al. (2019) suggest that the
605 steepest structural gradients and greatest uplift, towards the centre of fault segments drive the location
606 of primary sediment input points on dip slopes, whereas shallower structural gradients around fault tips
607 are more likely to be easily transgressed by rising sea level and sediment starved. Our findings indicate
608 that, in addition to structural changes, the width and bedrock composition of the dip slope are important
609 factors to consider in controlling sediment supply, the nature of the dip slope coastal plain, and shallow
610 marine regime. Narrow exposed zones of dip slopes, without the development of drainage catchments,
611 may not be able to contribute significant sediment yield in order to build constructive coastlines (**Figure**
612 **15a**). Broader dip slopes can develop larger catchments and potentially connect to greater altitudinal
613 differences from headwaters to drainage outlet, with consequently greater discharge and erosional
614 capability from steeper drainage profiles (Sømme et al., 2009; Romans et al., 2016; Nyberg et al., 2018).
615 dip slope Nevertheless, the sediment yield is likely to be relatively small given the shallow angle of dip
616 slopes (0-7°, Muravchik et al., 2018) compared to steeper catchment systems developed on the footwall
617 scarp of normal. Slower subsidence rates, shallower gradients and shallow water depths make dip
618 slope systems prone to be constructional depositional systems unlike steep, deep fault-attached
619 systems in the immediate hangingwall of major normal faults (Gawthorpe et al., 1994; Ravnås & Steel,
620 1998; Rapozo et al., 2021; Smyrak-Sikora et al., 2021). For example, the Viking Group in the
621 hangingwall of the major faults (KFC and VFC) that bound the Frøya High are dominated by deep-water
622 fans and bypassed fault scarps with limited capacity for shelfal development or shoreline sediment
623 storage (Elliot et al., 2015, 2017; Jones et al., 2020). The tectonostratigraphic setting of constructive
624 shorelines on the low gradient, back-tilted footwall dip slopes may record substantially different
625 stratigraphic architecture and depositional stacking patterns due to their increased sensitivity to eustatic
626 base-level changes compared to depositional systems in the immediate hangingwall of a major normal
627 fault (Leeder & Jackson, 1993; Gawthorpe et al., 1994, 2017; Ravnås & Steel., 1998; Jackson et al.,
628 2005; Henstra et al., 2017; Barrett et al., 2018; Smyrak-Sikora et al., 2021). dip slope

629 **9.2.2 Impact of the structural configuration of dip slope systems**

630

631 Other dip slope systems (e.g. El-Qaa and Hammam Faraun Fault Blocks, Gulf of Suez (Jackson et al.,
632 2005; Muravchik et al., 2018); Snorre-H area and, Central Graben of the North Sea (Nøttvedt et al.,
633 2000); Upper Heather Member, Oseberg Fault Block (Ravnås et al., 1997; Ravnås & Steel., 1998)), all
634 exhibit a net-transgressive character from drowning of the dip slope similar to the capping of the deltas
635 here by a transgressive section (**Figure 9**). Large scale, terminal flooding occurs because of continued
636 rotation and net subsidence of the dip slope in response to either to background-subsidence of the
637 margin and cessation of fault, or enhanced activity in the hangingwall of a nearby fault (e.g., Ravnås et
638 al., 1997; Ravnås & Steel., 1998). Unlike other published examples, all the clinofolds observed on the
639 Frøya High show strongly progradational character, and we observe no backstepping of deltaic units at
640 the seismic scale prior to their termination. Observations in 6306/9-1 demonstrate a well-developed
641 delta topset which is abruptly flooded with a thin transgressive-lag overlain by offshore mudstones of
642 the Spekk Formation, rather than more gradual backstepping (**Figure 9**). This lack of protracted,
643 terminal retrogradation suggests flooding occurred abruptly due to rapid sea-level rise or drastic
644 sediment supply reduction, which would be counter intuitive against the ongoing uplift-induced
645 steepening of the catchment headwaters. The Abrupt transgression of the Frøya dip slope systems may
646 be at least partly explained through the drainage capture from headward erosion by catchments on the
647 Klakk Fault Complex footwall crest (**Figure 15a**). The Early Cretaceous timing of drainage capture to
648 south/southwest draining catchments is simultaneous with previously documented acceleration and
649 localisation of deformation on the Klakk Fault Complex due to its linkage to a major detachment in the
650 lower crust (Peron-Pinvidic et al., 2013; Bell et al., 2014; Muñoz-Barrera et al., 2020). The process of
651 drainage capture by footwall scarp drainage and reduction in dip slope catchment area may be a
652 common rearrangement where displacement on the controlling normal fault continues or accelerates
653 rather than transferring to other structures (Leeder et al., 2005; Privat et al., 2021).

654 To maintain progradational architectures without retrogradation during net subsidence however
655 requires substantial sediment flux. The balance of sediment supply to accommodation for dip slope
656 depositional systems will be influenced by rotation of the fault block, uplift of the catchment to steepen
657 drainage profiles, the gradient of the subsiding (depositional) part of the dip slope, and any changes in
658 sea-level (Gawthorpe et al., 1994; Ravnås et al., 1997; Ravnås & Steel., 1998). Dip slopes in rift basins
659 can occur through two relationships to an active normal fault; rotation in the footwall of a major active
660 fault (**Figure 15a**), or rotation in the hangingwall of a major active fault (**Figure 15b**). In a footwall uplift
661 driven system such as the Frøya High, we observe strongly progradational architectures on the dip
662 slope prior to an abrupt termination of the system from drainage capture and flooding rather than the
663 preservation of a gradual retrogradation and transgression of the clinofold packages. The existence of
664 deltaic systems on the Frøya High in a depocenter approximately 20 km from the drainage divide, and
665 30 km from the Klakk Fault Complex, is consistent with a change to net-subsidence, due to contributions
666 from background subsidence, at half the wavelength of flexure of most large normal faults (40-60 km;
667 Morley, 1995; Armijo et al., 1996; Fernández-Blanco et al., 2020). Given the decay of uplift to
668 subsidence away from a bounding fault across a dip slope, the uplift of a dip slope catchment closer to
669 the fault is likely to be greater than the subsidence experienced in the dip slope further from the fault.
670 The resultant uplift-induced steepening of the drainage profile in the upper reaches of catchments, is

671 therefore likely to allow an increase in sediment flux which can exceed the accommodation generated
672 by subsidence to produce the strongly aggradational to progradational character observed on the Frøya
673 High dip slope (**Figure 15a**). Conversely, in a hangingwall subsidence driven setting (e.g., Alkyonides
674 Gulf – Leeder et al., 2005; El-Qaa Fault Block – Muravchik et al., 2018) (**Figure 15b**), subsidence is
675 likely to be greater in the depocentre than uplift in the catchment feeding the dip slope depositional
676 systems and uplift and steepening of the catchments may be very minor, or the catchment may even
677 undergo net subsidence (Pechlivanidou et al., 2019). As a result, even coastal systems with a fluvial
678 input become accommodation-dominated and are easily transgressed by subsidence-induced sea-level
679 increases producing the retrograding stacking patterns observed in hangingwall subsidence driven dip
680 slope systems such as those seen in the dip slope systems of the Alkyonides Gulf (Leeder et al., 2005),
681 Oseberg Fault Block (Ravnås et al., 1997; Ravnås & Steel., 1998) and El-Qaa and Hammam Faraun
682 Fault Blocks (Jackson et al., 2005; Muravchik et al., 2018). Temporal changes in fault activity (similar
683 to the high and low 'tilt rates' of Ravnås & Steel., 1998) , and interactions with non-tectonic changes in
684 sea-level or sediment flux have the capacity to alter this motif however the differences between
685 hangingwall and footwall driven dipslope systems highlights that the location of synchronous fault
686 activity is a key controlling parameter on evolution and resultant stacking patterns.

687 **10 Conclusions**

688 Detailed seismic mapping and analysis of borehole data within the Viking Group in the footwall dip
689 slope of the Klakk Fault Complex has revealed a constructive, delta-dominated shoreline system on the
690 eastern flank of the Frøya High. These sedimentary systems are sourced from eroded material from
691 the eastern side of a drainage divide in the footwall of the Klakk Fault Complex that was transported
692 eastwards down the back-tilted, footwall dip slope into the Froan Basin. This case study provides an
693 example of the facies and stratigraphic architecture of dip slope depositional systems within rift settings
694 and highlights spatial variations in dip slope sedimentation over 100 km along-strike.

695 The example on the Frøya High demonstrates the potential for intra-basinal highs to provide substantial
696 sediment sources not only into the hangingwall of major faults, but also across the back-tilted dip slope
697 in their footwall. Comparison with previous interpretations, and other examples of syn-rift dip slope
698 systems, highlight the likely transient nature of coarse-grained systems on dip slopes as they respond
699 to steepening of the headwaters of feeding catchments, which can drive high sediment flux and
700 progradation despite ongoing subsidence further down the dip slope. We hypothesise that footwall uplift
701 driven systems are likely to be more prone to progradation followed by abrupt shutdown resulting from
702 drainage capture by footwall scarp drainage networks. In contrast, hangingwall driven systems are more
703 prone to gradual transgression and form overall retrograding systems.

704 Integration with regional palaeogeography highlights that the deltaic packages may be important for
705 determining the location, sediment budget and calibre of sediment supplied to longshore shallow marine
706 systems such as spits and sand-ridges such as the Draugen Ridge. The study ultimately highlights
707 major progradation of dip slope systems on the back-tilted footwall dip slopes of intra-basinal highs
708 bound by high displacement normal faults, especially where bedrock is composed of easily erodible
709 material. This is in contrast to shallower gradient low-displacement dip slope systems, or those

710 generated in the hangingwall of large structures, which generally have more limited progradation, and
711 preserve strong retrogradational stacking patterns.

712 **11 Acknowledgements**

713 This research was conducted as part of the Petromaks II Syn-Rift Systems project (255229) funded by
714 the Norwegian Research Council and project partners (Equinor, ConocoPhillips, DNO, Neptune Energy,
715 AkerBP and Tullow Oil). AkerBP and former Lundin Energy are thanked for permission to publish data
716 from the 6306/9-1 well. We thank the reviewers Jonathan Obrist, Aleksandra Smyrak-Sikora and Lise
717 Nakken for their thorough, insightful, and constructive reviews and Cari Johnson for their editorial
718 handling of the manuscript. The authors thank Sander H Berg for discussion during the work in this
719 manuscript. Publically released data is accessed through the UiB-DISKOS agreement. RLG thanks the
720 VISTA programme of Norwegian Academy of Science and Letters for the award of its VISTA
721 Professorship. GAH is now an employee of AkerBP. There are no other conflicts of interest to declare.

722 **12 References**

- 723 Abbink, O., Targarona, J., Brinkhuis, H. and Visscher, H. 2001. Late Jurassic to earliest Cretaceous
724 palaeoclimatic evolution of the southern North Sea. *Global and Planetary Change*. 30(3), pp.231–256.
- 725 Anell, I., Zuchuat, V., Röhnert, A.D., Smyrak-Sikora, A., Buckley, S., Lord, G., Maher, H., Midtkandal,
726 I., Ogata, K., Olausson, S., Osmundsen, P.T. and Braathen, A. 2021. Tidal amplification and along-
727 strike process variability in a mixed-energy paralic system prograding onto a low accommodation shelf,
728 Edgeøya, Svalbard. *Basin Research*. 33(1), pp.478–512.
- 729 Armijo, R., Meyer, B., King, G.C.P., Rigo, A. and Papanastassiou, D. 1996. Quaternary evolution of the
730 Corinth Rift and its implications for the Late Cenozoic evolution of the Aegean. *Geophysical Journal
731 International*. 126(1), pp.11–53.
- 732 Ashcroft, W. 2011. Chapter Six: Velocity analysis, CMP stacking and post-stack migration *in: A
733 Petroleum Geologist's Guide to Seismic Reflection*. Blackwell Publishing. pp 41 – 49.
- 734 Backert, N., Ford, M. and Malartre, F. 2010. Architecture and sedimentology of the Kerinitis Gilbert-type
735 fan delta, Corinth Rift, Greece. *Sedimentology*. 57(2), pp.543–586.
- 736 Barrett, B.J., Hodgson, D.M., Collier, R.E.L. and Dorrell, R.M. 2018. Novel 3D sequence stratigraphic
737 numerical model for syn-rift basins: Analysing architectural responses to eustasy, sedimentation and
738 tectonics. *Marine and Petroleum Geology*. 92, pp.270–284.
- 739 Barrett, B.J., Collier, R.E.L., Hodgson, D.M., Gawthorpe, R.L., Dorrell, R.M. and Cullen, T.M. 2019.
740 Quantifying faulting and base level controls on syn-rift sedimentation using stratigraphic architectures
741 of coeval, adjacent Early-Middle Pleistocene fan deltas in Lake Corinth, Greece. *Basin Research*. 31(6),
742 pp.1040–1065.
- 743 Barrett, B.J., Hodgson, D.M., Jackson, C.A.-L., Lloyd, C., Casagrande, J. and Collier, R.E.L. 2021.
744 Quantitative analysis of a footwall-scarp degradation complex and syn-rift stratigraphic architecture,
745 Exmouth Plateau, NW Shelf, offshore Australia. *Basin Research*. 33(2), pp.1135–1169.
- 746 Bilal, A., McClay, K. and Scarselli, N. 2020. Fault-scarp degradation in the central Exmouth Plateau,
747 North West Shelf, Australia. *In: McClay, K.R & Hammerstein, J.A (eds) Passive Margins: Tectonics,
748 Sedimentation and Magmatism. Geological Society, London, Special Publications no. 476(1)*, pp.231–
749 257. Biscara, L., Hanquiez, V., Leynaud, D., Marieu, V., Mulder, T., Gallissaires, J.-M., Crespín, J.-P.,
750 Braccini, E. and Garlan, T. 2012. Submarine slide initiation and evolution offshore Pointe Odden, Gabon
751 — Analysis from annual bathymetric data (2004–2009). *Marine Geology*. 299–302, pp.43–50.

- 752 Beckers, A., Hubert-Ferrari, A., Beck, C., Papatheodorou, G., de Batist, M., Sakellariou, D., Tripsanas,
753 E. and Demoulin, A. 2018. Characteristics and frequency of large submarine landslides at the western
754 tip of the Gulf of Corinth. *Natural Hazards and Earth System Sciences*. 18(5), pp.1411–1425.
- 755 Bell, R.E., Jackson, C. a.-L., Elliott, G.M., Gawthorpe, R.L., Sharp, I.R. and Michelsen, L. 2014. Insights
756 into the development of major rift-related unconformities from geologically constrained subsidence
757 modelling: Halten Terrace, offshore mid Norway. *Basin Research*. 26(1), pp.203–224.
- 758 Bell, R.E., Duclaux, G., Nixon, C.W., Gawthorpe, R.L. and McNeill, L.C. 2017. High-angle, not low-
759 angle, normal faults dominate early rift extension in the Corinth Rift, central Greece. *Geology*. 46(2),
760 pp.115–118.
- 761 Berne, S., Lericolais, G., Marsset, T., Bourillet, J.F. and De Batist, M. 1998. Erosional offshore sand
762 ridges and lowstand shorefaces; examples from tide- and wave-dominated environments of France.
763 *Journal of Sedimentary Research*. 68(4), pp.540–555.
- 764 Blystad, P., Brekke, H., Færseth, R.B., Larsen, B.T., Skogseid, J. and Tørudbakken, B. 1995. Structural
765 elements of the Norwegian continental shelf. Part II: The Norwegian Sea Region. The Norwegian
766 Petroleum Directorate.
- 767 Brekke, H. and Riis, F. 1987. Tectonics and basin evolution of the Norwegian shelf between 62°N and
768 72°N. *Norsk Geologisk Tidsskrift*. 67, pp.295–322.
- 769 Brekke, H. 2000. The tectonic evolution of the Norwegian Sea Continental Margin with emphasis on the
770 Vøring and Møre Basins In: A. Nøttvedt, B. T. Larsen, S. Olaussen, B. Tørudbakken, J. Skogseid, R.
771 H. Gabrielsen, H. Brekke and Ø. Birkeland, eds. *Dynamics of the Norwegian Margin Geological Society*
772 *Special Publication No. 167*: Geological Society of London, pp.327–378.
- 773 Brekke, H., Dahlgren, S., Nyland, B. and Magnus, C. 1999. The prospectivity of the Vøring and Møre
774 basins on the Norwegian Sea continental margin. *Geological Society, London, Petroleum Geology*
775 *Conference series*. 5(1), pp.261–274.
- 776 Bunkholt, H.S.S., Oftedal, B.T., Hansen, J.A., Løseth, H. and Kløvjan, O.S. 2022. Trøndelag Platform
777 and Halten–Dønna Terraces Composite Tectono-Sedimentary Element, Norwegian Rifted Margin,
778 Norwegian Sea. In: Drachev, S.S., Brekke, H., Henriksen, E., Moore, T (eds.) *Sedimentary Succession*
779 *of the Arctic Region and their Hydrocarbon Prospectivity, Geological Society, London, Memoirs*. 57(1),
780 pp.M57-2017–13. Chiarella, D., Longhitano, S.G., Mosdell, W. and Telesca, D. 2020. Sedimentology
781 and facies analysis of ancient sand ridges: Jurassic Rogn Formation, Trøndelag Platform, offshore
782 Norway. *Marine and Petroleum Geology*. 112, p.104082.
- 783 Corfield, S., Sharp, I., Häger, K.-O., Dreyer, T. and Underhill, J. 2001. An integrated study of the Garn
784 and Melke formations (Middle to Upper jurassic) of the Smorbukk area, Halten terrace, mid-Norway In:
785 O. J. Martinsen and T. Dreyer, eds. *Norwegian Petroleum Society Special Publications. Sedimentary*
786 *Environments Offshore Norway — Palaeozoic to Recent* pp.199–210.
- 787 Coward, M.P., Dewey, J.F., Hempton, M., and J Holroyd 2003. Tectonic evolution In: D. Evans, C.
788 Graham, A. Armour and P. Bathurst, eds. *The Millennium Atlas: Petroleum Geology of the Central and*
789 *Northern North Sea*. The Geological Society of London, pp.17–33.
- 790 Elliott, G.M., Jackson, C.A.-L., Gawthorpe, R.L., Wilson, P., Sharp, I.R. and Michelsen, L. 2017. Late
791 syn-rift evolution of the Vingleia Fault Complex, Halten Terrace, offshore Mid-Norway; a test of rift basin
792 tectono-stratigraphic models. *Basin Research*. 29(S1), pp.465–487.
- 793 Elliott, G.M., Jackson, C.A.-L., Gawthorpe, R.L., Wilson, P., Sharp, I.R. and Michelsen, L. 2021.
794 Tectono-stratigraphic development of a salt-influenced rift margin: Halten Terrace, offshore Mid-
795 Norway. *Basin Research*. 33(6), pp.3295–3320. Eliet, P.P., Gawthorpe, R.L. 1995. Drainage
796 development and sediment supply within rifts, examples from the Sperchios basin, central Greece.
797 *Journal of the Geological Society, London*. 152. pp. 883-893.

- 798 Færseth, R.B. 1996. Interaction of Permo-Triassic and Jurassic extensional fault-blocks during the
799 development of the northern North Sea. *Journal of the Geological Society*. 153(6), pp.931–944.
- 800 Færseth, R.B. 2021. Structural geology and basin development of the Norwegian Sea. *Norwegian*
801 *Journal of Geology*. 100, 202018
- 802 Fernández-Blanco, D., Gelder, G. de, Lacassin, R. and Armijo, R. 2020. Geometry of Flexural Uplift by
803 Continental Rifting in Corinth, Greece. *Tectonics*. 39(1), e2019TC005685.
- 804 Gales, J.A., Talling, P.J., Cartigny, M.J.B., Clarke, J.H., Lintern, G., Stacey, C. and Clare, M.A. 2019.
805 What controls submarine channel development and the morphology of deltas entering deep-water
806 fjords? *Earth Surface Processes and Landforms*. 44(2), pp.535–551.
- 807 Gawthorpe, R.L. and Leeder, M.R. 2000. Tectono-sedimentary evolution of active extensional basins.
808 *Basin Research*. 12(3–4), pp.195–218.
- 809 Gawthorpe, R.L., Fraser, A.J. and Collier, R.E.L.I. 1994. Sequence stratigraphy in active extensional
810 basins: implications for the interpretation of ancient basin-fills. *Marine and Petroleum Geology*. 11(6),
811 pp.642–658.
- 812 Gawthorpe, R.L., Andrews, J.E., Collier, R.E.L., Ford, M., Henstra, G.A., Kranis, H., Leeder, M.R.,
813 Muravchik, M. and Skourtsos, E. 2017. Building up or out? Disparate sequence architectures along an
814 active rift margin—Corinth rift, Greece. *Geology*. 45(12), pp.1111–1114.
- 815 Gawthorpe, R.L., Leeder, M.R., Kranis, H., Skourtsos, E., Andrews, J.E., Henstra, G.A., Mack, G.H.,
816 Muravchik, M., Turner, J.A. and Stamatakis, M. 2018. Tectono-sedimentary evolution of the Plio-
817 Pleistocene Corinth rift, Greece. *Basin Research*. 30(3), pp.448–479.
- 818 Gernigon, L., Franke, D., Geoffroy, L., Schiffer, C., Foulger, G.R. and Stoker, M. 2020. Crustal
819 fragmentation, magmatism, and the diachronous opening of the Norwegian-Greenland Sea. *Earth-*
820 *Science Reviews*. 206, p.102839.
- 821 Gobo, K., Ghinassi, M. and Nemec, W. 2014. Reciprocal Changes In Foreset To Bottomset Facies In
822 A Gilbert-Type Delta: Response To Short-Term Changes In Base Level. *Journal of Sedimentary*
823 *Research*. 84(11), pp.1079–1095.
- 824 Gastaldo, R.A and Huc, A-Y. 1992. Sediment Facies, Depositional Environments, and Distribution of
825 Phytoclasts in the Recent Mahakam River Delta, Kalimantan, Indonesia. *Palaeos*. 7(6) pp. 574-590.
- 826 Gradstein, F.M., Anthonissen, E., Brunstad, H., Charnock, M., Hammer, O., Hellem, T., Lervik, K.S.,
827 Norwegian offshore Stratigraphic Lexicon (NORLEX). 2010 *Newsletters on Stratigraphy* 44. pp73-86
- 828 Gradstein, F. 2017. Lundin Norway lithostratigraphic charts. Available online at
829 https://timescalefoundation.org/resources/NW_Europe_Lex/stratchart.php
- 830 Grunnaleite, I. and Gabrielsen, R.H. 1995. Structure of the Møre basin, mid-Norway continental margin.
831 *Tectonophysics*. 252(1), pp.221–251.
- 832 Halland, E.K., Bjørnstad, A., Magnus, C., Riis, F., Meling, I.M., Gjeldvik, I.T., Tappel, I.M., Mujezinović,
833 J., Bjørheim, M., Rød, R.S. and Pham, V.T.H. 2014. 5. The Norwegian Sea In: *CO₂ Storage Atlas:*
834 *Norwegian Continental Shelf. Stavanger, Norway: Norwegian Petroleum Directorate (NPD)*, pp.75–105.
- 835 Henstra, G.A., Gawthorpe, R.L., Helland-Hansen, W., Ravnås, R. and Rotevatn, A. 2017. Depositional
836 systems in multiphase rifts: seismic case study from the Lofoten margin, Norway. *Basin Research*.
837 29(4), pp.447–469.
- 838 Hovius, N. 1996. Regular spacing of drainage outlets from linear mountain belts. *Basin Research*. 8 (1).
839 pp 29-44
- 840 Jackson, C.A.L., Gawthorpe, R.L., Carr, I.D., Sharp, I.R. 2005. Normal faulting as a control on the
841 stratigraphic development of shallow marine syn-rift sequences: the Nukhul and Lower Rudeis
842 Formations, Hammam Faraun fault block, Suez Rift, Egypt. *Sedimentology*. 52. pp. 313-338.

- 843 Johnson, P.W and Hansen, K. 1987. Method for Calibrating Stacking Velocities for Use in Time-Depth
844 Conversion. *19th Annual Offshore Technology Conference*. Houston, Texas, April 27-30.
- 845 Jones, G.E.D., Welbon, A.I.F., Mohammadlou, H., Sakharov, A., Ford, J., Needham, T. and Ottesen,
846 C. 2021. Complex stratigraphic fill of a small, confined syn-rift basins: an Upper Jurassic example from
847 offshore mid-Norway *In: D. Chiarella, S. G. Archer, J. A. Howell, C. A. L. Jackson, H. Kombrink and S.*
848 *Patruno, eds. Cross-Border Themes in Petroleum Geology II: Atlantic Margin and Barents Sea*
849 *Geological Society Special Publication No. 495: Geological Society of London.*
- 850 Jongepier, K., Rui, J.C. and Grue, K. 1996. Triassic to Early Cretaceous stratigraphic and structural
851 development of the northeastern Møre Basin margin, off Mid-Norway. *Norsk Geologisk Tidsskrift.*, p.17.
- 852 Leeder, M.R. and Jackson, J.A. 1993. The interaction between normal faulting and drainage in active
853 extensional basins, with examples from the western United States and central Greece. *Basin Research.*
854 5(2), pp.79–102.
- 855 Leeder, M.R., Portman, C., Andrews, J.E., Collier, R.E.LI., Finch, E., Gawthorpe, R.L., McNeill, L.C.,
856 Pérez-Arlucea, M. and Rowe, P. 2005. Normal faulting and crustal deformation, Alkyonides Gulf and
857 Perachora Peninsula, eastern Gulf of Corinth rift, Greece. *Journal of the Geological Society.* 162(3),
858 pp.549–561.
- 859 Marsden, D. 1989. Layer cake depth conversion, Part I. *The Leading Edge.* 8. 10-14.
- 860 Martinius, A.W., Kaas, I., Næss, A., Helgesen, G., Kjærefjord, J.M. and Leith, D.A. 2001. Sedimentology
861 of the heterolithic and tide-dominated tilje formation (Early Jurassic, Halten Terrace, Offshore Mid-
862 Norway) *In: O. J. Martinsen and T. Dreyer, eds. Sedimentary Environments Offshore Norway —*
863 *Palaeozoic to Recent Norwegian Petroleum Society Special Publications* pp.103–144.
- 864 Massari F., Colella A. 1988. Evolution and types of fan-delta systems in some major tectonic settings.
865 *In Nemeč W., Steel R.J. (Eds.), Fan Deltas: Sedimentology and Tectonic Settings*, Blackie, Glasgow
866 pp. 103-122
- 867 Mjelde, R., Faleide, J.I., Breivik, A.J. and Raum, T. 2009. Lower crustal composition and crustal
868 lineaments on the Vøring Margin, NE Atlantic: A review. *Tectonophysics.* 472(1), pp.183–193.
- 869 Mørk, M.B.E. and Johnsen, S.O. 2005. Jurassic sandstone provenance and basement erosion in the
870 Møre margin – Froan Basin area. *NGU Bulletin.* 443, p.14.
- 871 Morley, C.K. and Lambiase, J.J. 1995. Developments in the structural geology of rifts over the last
872 decade and their impact on hydrocarbon exploration *In Lambiase, J.J eds. Hydrocarbon Habitat in Rift*
873 *Basins, Geological Society Special Publication No. 80.* Geological Society of London, pp.1–32.
- 874 Muñoz-Barrera, J.M., Rotevatn, A., Gawthorpe, R.L., Henstra, G.A. and Kristensen, T.B. 2020. The role
875 of structural inheritance in the development of high-displacement crustal faults in the necking domain
876 of rifted margins: The Klakk Fault Complex, Frøya High, offshore mid-Norway. *Journal of Structural*
877 *Geology.* 140, p.104163.
- 878 Muñoz-Barrera, J. M., Rotevatn, A., Gawthorpe, R.L., Henstra, G., & Kristensen, T.
879 B. 2022. Supradetachment basins in necking domains of rifted margins: Insights from the Norwegian
880 Sea. *Basin Research*, 34, 991– 1019. <https://doi.org/10.1111/bre.12648>
- 881 Muravchik, M., Gawthorpe, R.L., Sharp, I.R., Rarity, F. and Hodgetts, D. 2018. Sedimentary
882 environment evolution in a marine hangingwall dip slope setting. El Qaa Fault Block, Suez Rift, Egypt.
883 *Basin Research.* 30(S1), pp.452–478.
- 884 Mutterlose, J., Brumsack, H., Flögel, S., Hay, W., Klein, C., Langrock, U., Lipinski, M., Ricken, W.,
885 Söding, E., Stein, R. and Swientek, O. 2003. The Greenland-Norwegian Seaway: A key area for
886 understanding Late Jurassic to Early Cretaceous paleoenvironments. *Paleoceanography.* 18(1).
- 887 Nemeč, W. 1990. Aspects of Sediment Movement on Steep Delta Slopes *In: A. Colella and D. B. Prior,*
888 *eds. Coarse-Grained Deltas.* John Wiley & Sons, Ltd, pp.29–73.

- 889 Nielsen, L.H. and Johannessen, P.N. 2009. Facies architecture and depositional processes of the
890 Holocene–Recent accretionary forced regressive Skagen spit system, Denmark. *Sedimentology*. 56(4),
891 pp.935–968.
- 892 Nøttvedt, A., Berge, A.M., Dawers, N.H., Færseth, R.B., Häger, K.O., Mangerud, G. and
893 Puigdefabregas, C. 2000. Syn-rift evolution and resulting play models in the Snorre-H area, northern
894 North Sea *In: A Nøttvedt, B. T. Larsen, R. H. Gabrielsen, S. Olausen, H. Brekke, B. Tørudbakken, Ø.*
895 *Birkeland and J. Skogseid, eds. Dynamics of the Norwegian Margin, Geological Society, London,*
896 *Special Publication No. 167.* Geological Society of London, pp.179–218.
- 897 Nyberg, B., Helland-Hansen, W., Gawthorpe, R., Tillmans, F. and Sandbakken, P. 2021. Assessing
898 first-order BQART estimates for ancient source-to-sink mass budget calculations. *Basin Research*.
899 33(4), pp.2435–2452.
- 900 Olesen, O., Brønner, M., Ebbing, J., Gellein, J., Gernigon, L., Koziel, J., Lauritsen, T., Myklebust, R.,
901 Pascal, C., Sand, M., Solheim, D. and Usov, S. 2010. New aeromagnetic and gravity compilations from
902 Norway and adjacent areas: methods and applications. *Geological Society, London, Petroleum*
903 *Geology Conference series*. 7(1), pp.559–586.
- 904 Osmundsen, P.T. and Ebbing, J. 2008. Styles of extension offshore mid-Norway and implications for
905 mechanisms of crustal thinning at passive margins. *Tectonics*. 27(6).
- 906 Osmundsen, P.T. and Péron-Pinvidic, G. 2018. Crustal-Scale Fault Interaction at Rifted Margins and
907 the Formation of Domain-Bounding Breakaway Complexes: Insights From Offshore Norway. *Tectonics*.
908 37(3), pp.935–964.
- 909 Osmundsen, P.T., Péron-Pinvidic, G., Ebbing, J., Erratt, D., Fjellanger, E., Bergslien, D. and Syvertsen,
910 S.E. 2016. Extension, hyperextension and mantle exhumation offshore Norway: a discussion based on
911 6 crustal transects. *Norwegian Journal of Geology*. Pp. 343-372
- 912 Gernigon, L., Franke, D., Geoffroy, L., Schiffer, C., Foulger, G.R. and Stoker, M. 2020. Crustal
913 fragmentation, magmatism, and the diachronous opening of the Norwegian-Greenland Sea. *Earth-*
914 *Science Reviews*. 206, p.102839.
- 915 Patruno, S., Hampson, G.J., Jackson, C.A-L. 2015. Quantitative characterisation of deltaic and
916 subaqueous clinoforms. *Earth-Science Reviews*. 142. pp 79-119
- 917 Pechlivanidou, S., Cowie, P.A., Duclaux, G., Nixon, C.W., Gawthorpe, R.L. and Salles, T. 2019. Tipping
918 the balance: Shifts in sediment production in an active rift setting. *Geology*. 47(3), pp.259–262.
- 919 Peron-Pinvidic, G., Manatschal, G. and Osmundsen, P.T. 2013. Structural comparison of archetypal
920 Atlantic rifted margins: A review of observations and concepts. *Marine and Petroleum Geology*. 43,
921 pp.21–47.
- 922 Postma, G. 1984. Slumps and their deposits in fan delta front and slope. *Geology*. 12(1), pp.27–30.
- 923 Prior, D.B. and Bornhold, B.D. 1989. Submarine sedimentation on a developing Holocene fan delta.
924 *Sedimentology*. 36(6), pp.1053–1076.
- 925 Privat, A.M.-L.J., Hodgson, D.M., Jackson, C.A.-L., Schwarz, E. and Peakall, J.2021. Evolution from
926 syn-rift carbonates to early post-rift deep-marine intraslope lobes: The role of rift basin physiography on
927 sedimentation patterns. *Sedimentology*. *Online*
- 928 Rapozo, B.F., Córdoba, V.C. and Antunes, A.F. 2021. Tectono-stratigraphic evolution of a cretaceous
929 intracontinental rift: Example from Rio do Peixe Basin, north-eastern Brazil. *Marine and Petroleum*
930 *Geology*. 126, p.104899.
- 931 Ravnås, R., Bondevik, K., Helland-Hansen, W., Lømo, L., Ryseth, A and Steel, R.J. 1997.
932 Sedimentation history as an indicator of rift initiation and development: the Late Bajocian-Bathonian
933 evolution of the Oseberg-Brage area, northern North Sea. *Norsk Geologisk Tidsskrift*. 77. pp 205-232.

- 934 Ravnås, R. and Steel, R.J. 1998. Architecture of Marine Rift-Basin Successions. *AAPG Bulletin*. 82(1),
935 pp.110–146.
- 936 Roberts, A.M., Corfield, R.I., Kuszniir, N.J., Matthews, S.J., Hansen, E.-K. and Hooper, R.J. 2009.
937 Mapping palaeostructure and palaeobathymetry along the Norwegian Atlantic continental margin: Møre
938 and Vøring basins. *Petroleum Geoscience*. 15(1), pp.27–43.
- 939 Rohais, S., Eschard, R. and Guillocheau, F. 2008. Depositional model and stratigraphic architecture of
940 rift climax Gilbert-type fan deltas (Gulf of Corinth, Greece). *Sedimentary Geology*. 210(3), pp.132–145.
- 941 Romans, B.W., Castellort, S., Covault, J.A., Fildani, A. and Walsh, J.P. 2016. Environmental signal
942 propagation in sedimentary systems across timescales. *Earth-Science Reviews*. 153, pp.7–29.
- 943 Rossi, V.M. and Steel, R.J. 2016. The role of tidal, wave and river currents in the evolution of mixed-
944 energy deltas: Example from the Lajas Formation (Argentina). *Sedimentology*. 63(4), pp.824–864.
- 945 Rubi, R., Rohais, S., Bourquin, S., Moretti, I. and Desaubliaux, G. 2018. Processes and typology in
946 Gilbert-type delta bottomset deposits based on outcrop examples in the Corinth Rift. *Marine and
947 Petroleum Geology*. 92, pp.193–212.
- 948 Skarbø, O., Bakke, S., Jacobsen, T., Krokstad, W., Lundschieen, B., Myhr, M.B., Rise, L., Schou, L.,
949 Smelror, M., Verdenius, J.G., Vigran, J.O. & Århus, N. (1988) Shallow Drilling Off Møre-Trøndelag 1998,
950 IKU Sintef group, 387.
- 951 Smyrak-Sikora, A., Nicolaisen, J.B., Braathen, A., Johannessen, E.P., Olaussen, S. and Stemmerik, L.
952 2021. Impact of growth faults on mixed siliciclastic-carbonate-evaporite deposits during rift climax and
953 reorganisation—Billefjorden Trough, Svalbard, Norway. *Basin Research*. *Accepted Version Online*
- 954 Smyrak-Sikora, A., Johannessen, E.P., Olaussen, S., Sandal, G. and Braathen, A. 2018. Sedimentary
955 architecture during Carboniferous rift initiation – the arid Billefjorden Trough, Svalbard. *Journal of the
956 Geological Society*. 176(2), pp.225–252.
- 957 Sømme, T.O., Helland-Hansen, W., Martinsen, O.J. and Thurmond, J.B. 2009. Relationships between
958 morphological and sedimentological parameters in source-to-sink systems: a basis for predicting semi-
959 quantitative characteristics in subsurface systems. *Basin Research*. 21(4), pp.361–387.
- 960 Sømme, T.O., Jackson, C.A.L., Lunt, I., Martinsen, O. 2010. Source-to-Sink in Rift Basins – Predicting
961 Reservoir Distribution in Ancient, Subsurface Systems. *American Association of Petroleum Geologists
962 Annual Convention and Exhibition, New Orleans, Louisiana, USA, April 11-14 2010. Search and
963 Discovery article #10258*.
- 964 Statoil, 1994. Completion Report Well 6306/6-1 PL198 Harstad, Norway: Statoil. Available from:
965 [https://factpages.npd.no/pbl/wellbore_documents/2384_6306_6_1_COMPLETION_REPORT_AND_L
966 OG.pdf](https://factpages.npd.no/pbl/wellbore_documents/2384_6306_6_1_COMPLETION_REPORT_AND_LOG.pdf).
- 967 Talling, P.J., Stewart, M.D., Stark, C.P., Gupta, S., Vincent, S.J. 1997. Regular spacing of drainage
968 outlets from linear fault blocks. *Basin Research* 9. pp 275-302.
- 969 Van der Zwaan, C.J. 1990: Palynostratigraphy and Palynofacies Reconstruction of the Upper Jurassic
970 to Lowermost Cretaceous of the Draugen Field, Offshore Mid Norway. *Reviews of Palaeobotany and
971 Palynology* 62, 157-186 Wilson, P., Elliott, G.M., Gawthorpe, R.L., Jackson, C.A.-L., Michelsen, L. and
972 Sharp, I.R. 2015. Lateral variation in structural style along an evaporite-influenced rift fault system in
973 the Halten Terrace, Norway: Influence of basement structure and evaporite facies. *Journal of Structural
974 Geology*. 79, pp.110–123.
- 975 Wilson, P., Elliott, G.M., Gawthorpe, R.L., Jackson, C.A.-L., Michelsen, L. and Sharp, I.R. 2015. Lateral
976 variation in structural style along an evaporite-influenced rift fault system in the Halten Terrace, Norway:
977 Influence of basement structure and evaporite facies. *Journal of Structural Geology*. 79, pp.110–123..
- 978

979 **Figure 1:** A) Regional map of the key structural elements of the Norwegian Continental shelf offshore
980 Mid-Norway, After NPD (2022). SR – Sklinna Ridge, VFC – Vingleia Fault Complex, BFC – Bremmstein
981 Fault Complex. FF – Froan Fault B) Regional 2D seismic cross-section showing the location of the
982 Frøya High bound a high-displacement normal fault – the Klakk Fault Complex within the necking
983 domain of the Norwegian margin in this region. C) Inset of Frøya High regional section highlighting the
984 studied stratigraphy in the footwall of the Klakk Fault Complex.

985 **Figure 2:** **A)** Well-to-seismic tie for the stratigraphic interval of interest. A synthetic seismogram is
986 generated from the sonic and density logs of well 6306/6-1 (Location in Figure 1, 3). Key surfaces that
987 are recognised in the well are thus linked to their corresponding reflector in the seismic reflection survey
988 shown in **(B)**. **C)** Stratigraphic chart highlighting the lithostratigraphic nomenclature for the Norwegian
989 Margin in the Southern Norwegian Sea (modified from Gradstein et al., 2010 and Gradstein, 2017).
990 *TVD – True Vertical Depth, TWT – Two-Way Time, FH- Frøya High, SR – Sklinna Ridge, GH – Gossa
991 High. Tectonic events summarised from Bunkholt et al. (2022).

992 **Figure 3:** TWT structure maps of the three key surfaces; **A)** Top Basement, **B)** Base Viking Group and
993 **C)** Top Viking Group (BCU)) used in this study for isopachs and depositional system reconstruction.
994 Ticks on onlap extent lines point downdip towards deeper onlap.

995 **Figure 4:** Uninterpreted (A) and Interpreted (B) NW-SE trending seismic line intersecting Area A, E and
996 F highlighting the character of the Top Viking/BCU surface and Viking and Cromer Knoll Group
997 character in the area. Key truncation relationships are marked with arrows highlighting downlap within
998 the Viking Group in Area A, Onlap of the Cromer Knoll Group in Area F, and truncation of the Middle
999 Jurassic and Mesozoic stratigraphy by the Base Viking Group surface. Location and Areas are
1000 demonstrated in Figure 4.

1001 **Figure 5:** Isopach maps of A) Late Jurassic, Viking Group, generated by depth-converting and
1002 combining the base and top Viking Group TWT structure maps shown in Figures 3b and 3c,
1003 respectively. B) Early Cretaceous, Cromer Knoll Group, generated by depth converting and combining
1004 the top Viking Group TWT structure map (Figure. 3c) and an autotracked TWT surface of the base
1005 Shetland Group reflector. Key depocenters referred to in the text are labelled A, B, C, O – G.

1006 **Figure 6:** Uninterpreted (A) and interpreted (B) detailed seismic image of Viking Gp. wedge B
1007 intersection with well 6306/9-1 (Figure. 5a). Location shown in Figure 4. K – Cretaceous. J – Jurassic.
1008 Log within 6306/9-1 is provided in Figure 9. Yellow dots relate to the Top and Base of the Rogn
1009 Formation. Seismic sections are plotted in time and are not flattened to preserve the the true well path
1010 and allow the well log to be anchored on Top Viking and Top Basement reflectors.

1011 **Figure 7:** Non-flattened and Top Shetland Group flattened seismic sections through thickness
1012 anomalies of The Viking Group termed wedges B, C and C. All lines are west - left and east - right. A)
1013 Seismic line (unflattened and flattened) through Wedge A. B) Inset location map of cropped Viking
1014 Group thickness map, with seismic line locations (red lines). C) Seismic line (unflattened and flattened)
1015 through wedge C. D) Seismic line (unflattened and flattened) intersecting with 6306/6-1 through
1016 depocentre D. Erosional feature relates to Depocentre E in Figure 5b.

1017 **Figure 8:** Uninterpreted (A) and Interpreted (B) composite, approximately N-S oriented seismic lines
1018 with the three Viking Group wedges labelled. C, D) Insets of Wedge B and A respectively showing
1019 internal truncations and seismic character. Location shown in Figure 4.

1020 **Figure 9:** Summary well log for the Late Jurassic stratigraphy of 6306/9-1 compiled from wireline,
1021 sidewall core, biostratigraphic and borehole imaging observations. FMI – Formation Microresistivity
1022 Image, UBI – Ultrasonic Borehole Imager.

1023 **Figure 10.** A) Detail of Viking Group thickness map (Figure 4a) highlighting amphitheatre shaped
1024 depression bound by steep erosional scars within the eastern edge of Wedge A. Location on Figure 4.
1025 B) S (left) – N (right) oriented seismic line highlighting concave depressions within The Viking Group on
1026 the eastern edge of Wedge A. Location in part A.

1027 **Figure 11.** Cross sections demonstrating a simple restoration of the Top Viking Group/BCU structure
1028 map. The surface of **Figure 4c** is depth converted and rotated so that the areas interpreted to represent
1029 horizontal topsets of the deltaic clinoform packages A, B C, and D (Figure 12). Location in Figure 1a.

1030 **Figure 12.** Restored, depth converted, BCU structure map is based on rotation (Figure 11) to horizontal
1031 of the best-fit plane through the palaeo-horizontal topsets of the Upper Jurassic clinoform package. The
1032 resultant surface represents an approximation of the topography of the Frøya High at the end of the
1033 Jurassic. A-D – Deltaic clinoform packages. 1-4 – Deeply eroded areas.

1034 **Figure 13:** Simplified and interpretive palaeogeographic maps based on the distribution of stratigraphic
1035 packages and depositional environments as interpreted in the present study A) Generalised
1036 palaeogeographic reconstruction of the south-eastern part of the Frøya High and Froan Basin during
1037 the Late Jurassic deposition of deltaic clinoform packages (A,B,C) fed by catchments eroding from
1038 Triassic-Middle Jurassic subcrop (a,b,c). **B)** Generalised palaeogeographic reconstruction of the south-
1039 eastern part of the Frøya High and Froan Basin during the Early Cretaceous, forming substantial
1040 erosional systems, redirected to the south, compared to the eastern-draining systems during the Late
1041 Jurassic.

1042 **Figure 14:** A new, simple palaeogeographic model for the Late Jurassic deposition along the south-
1043 eastern margin of the Frøya High. The shoreline is supplied with abundant clastic material in the south,
1044 and potentially in the middle, and a longshore current connects it to the Draugen ridge that may
1045 represent a spit system rather than a detached sand ridge.

1046 **Figure 15:** Conceptual cartoons for evolutionary models of dip slope shoreline systems in A) A footwall
1047 uplift driven dip slope shoreline system. Here, progressive uplift in the footwall of a major fault drives
1048 sediment flux (T1 – T2) but also induces headward erosion from other catchments which capture dip
1049 slope drainage (T3). B) A hangingwall subsidence driven dip slope shoreline systems. Here,
1050 progressive subsidence in the hangingwall of a major fault drives a structural gradient to produce
1051 drainage catchments which are gradually transgressed (T2) and recorded as protracted shutdowns of
1052 shoreline systems (T3).

FIGURE 1

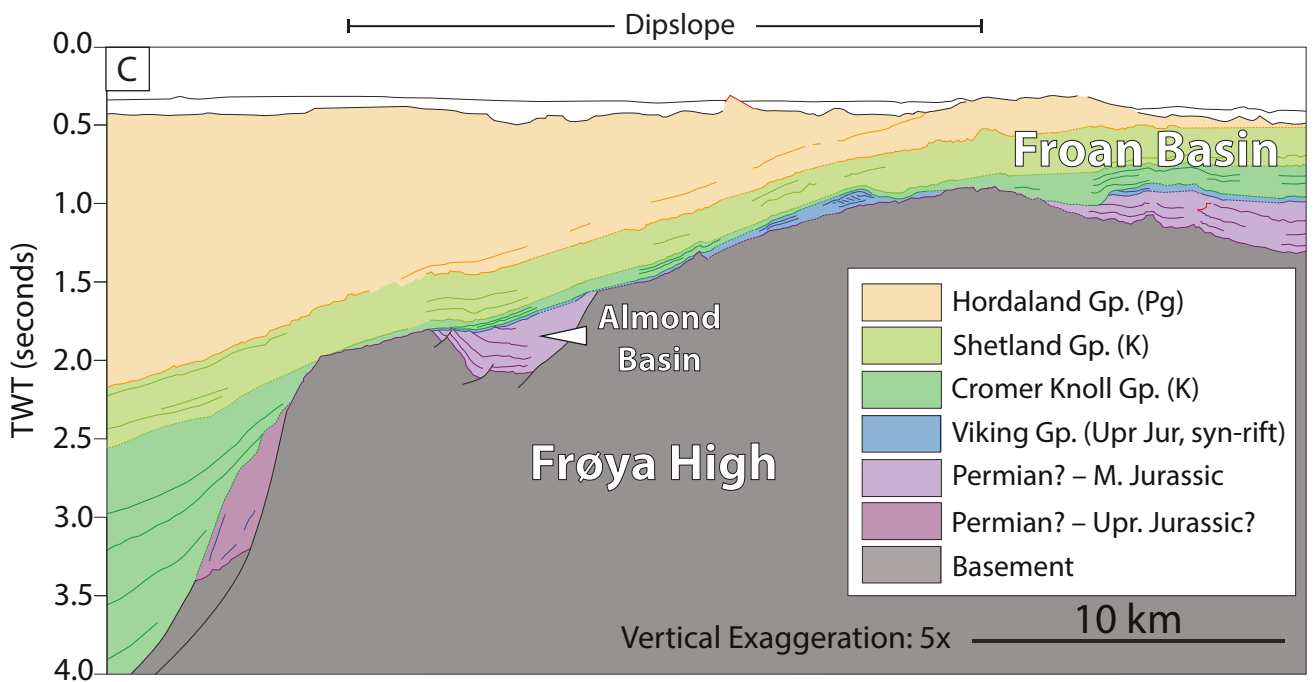
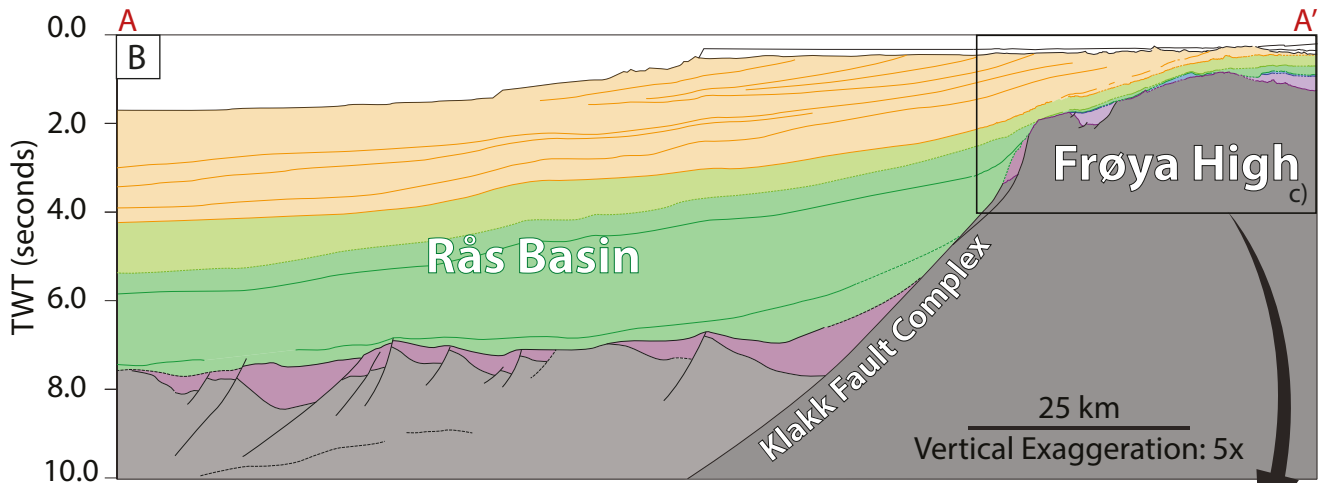
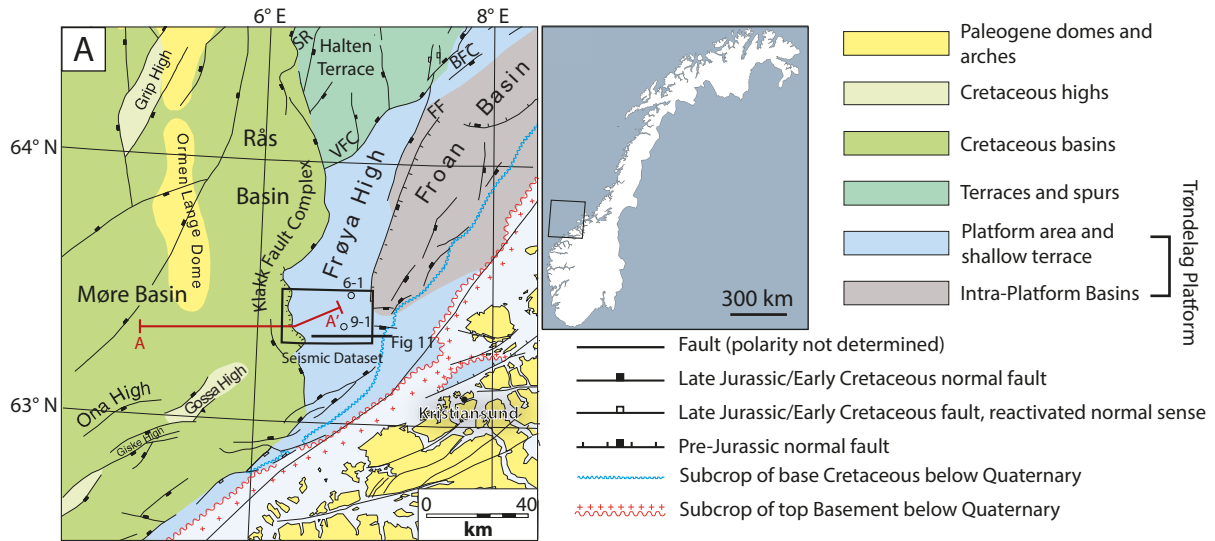


FIGURE 2

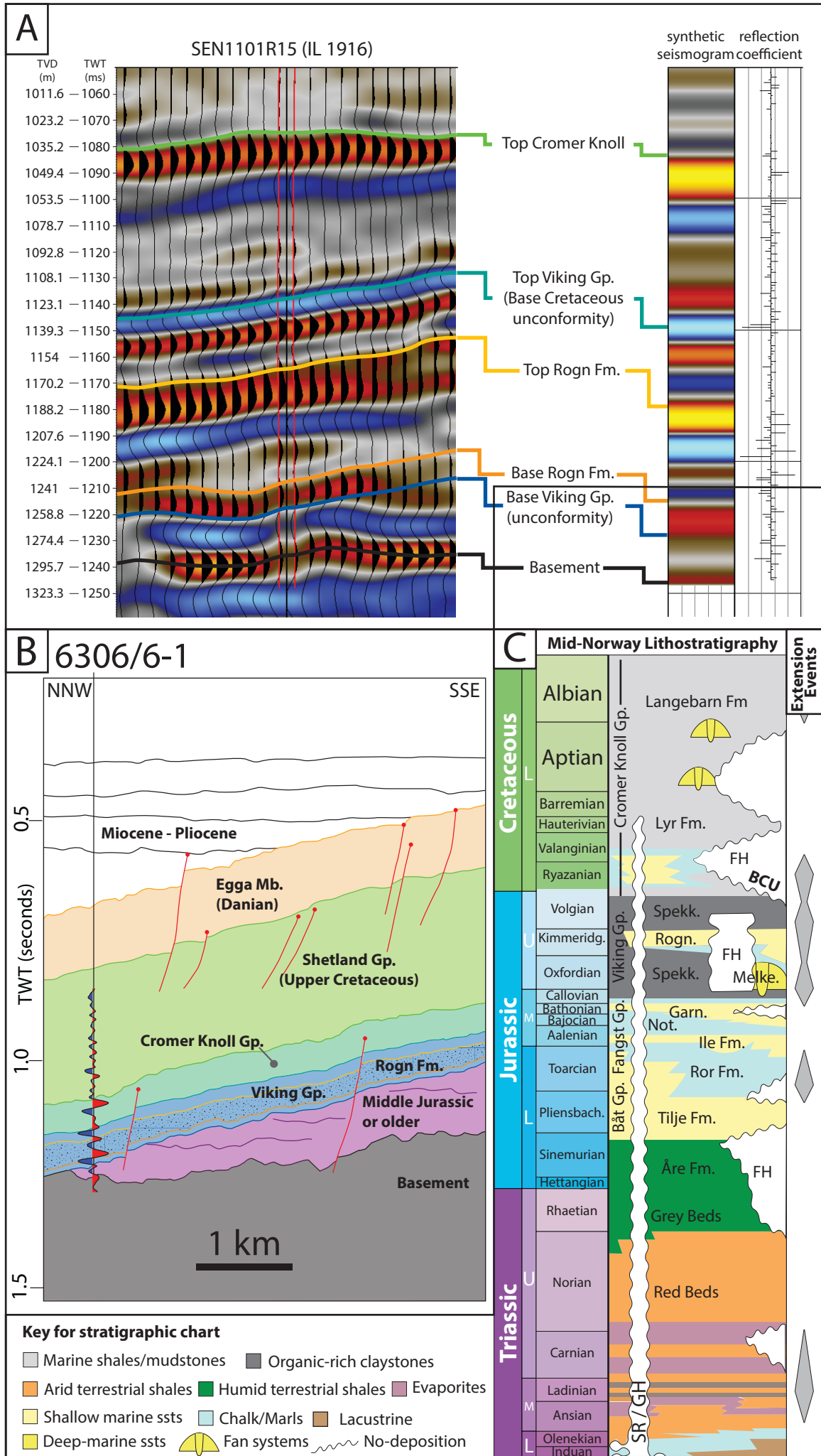


FIGURE 3

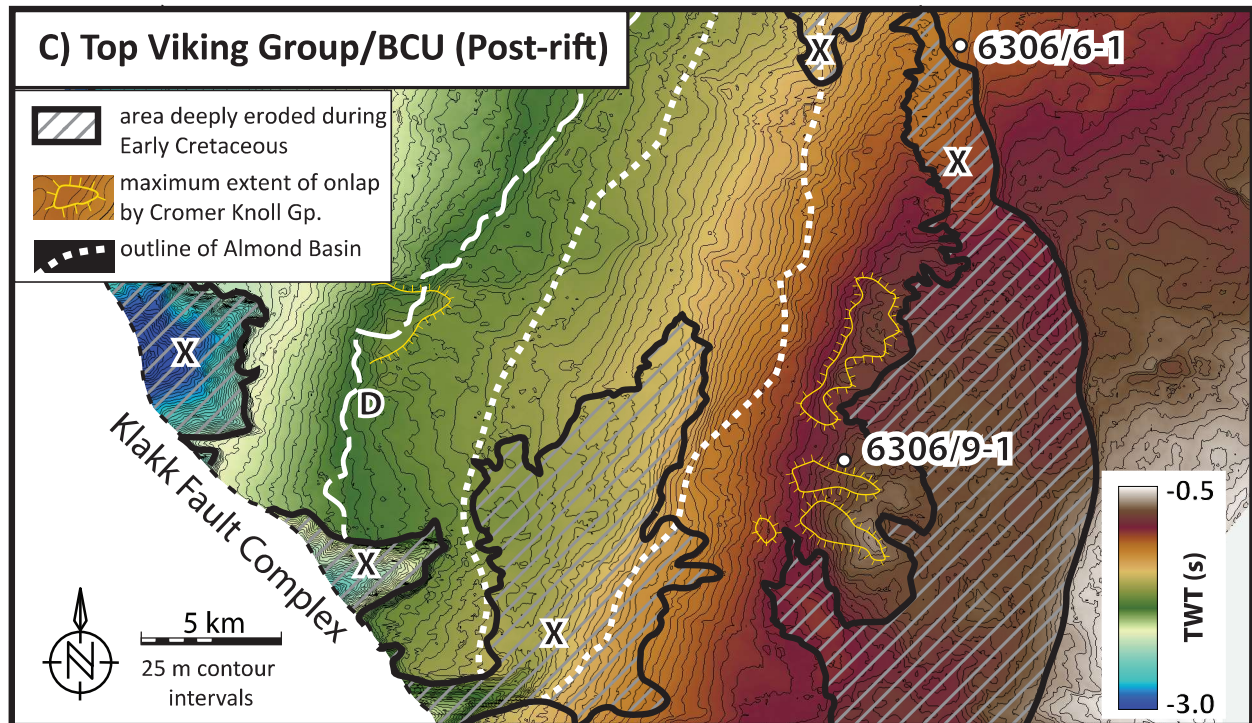
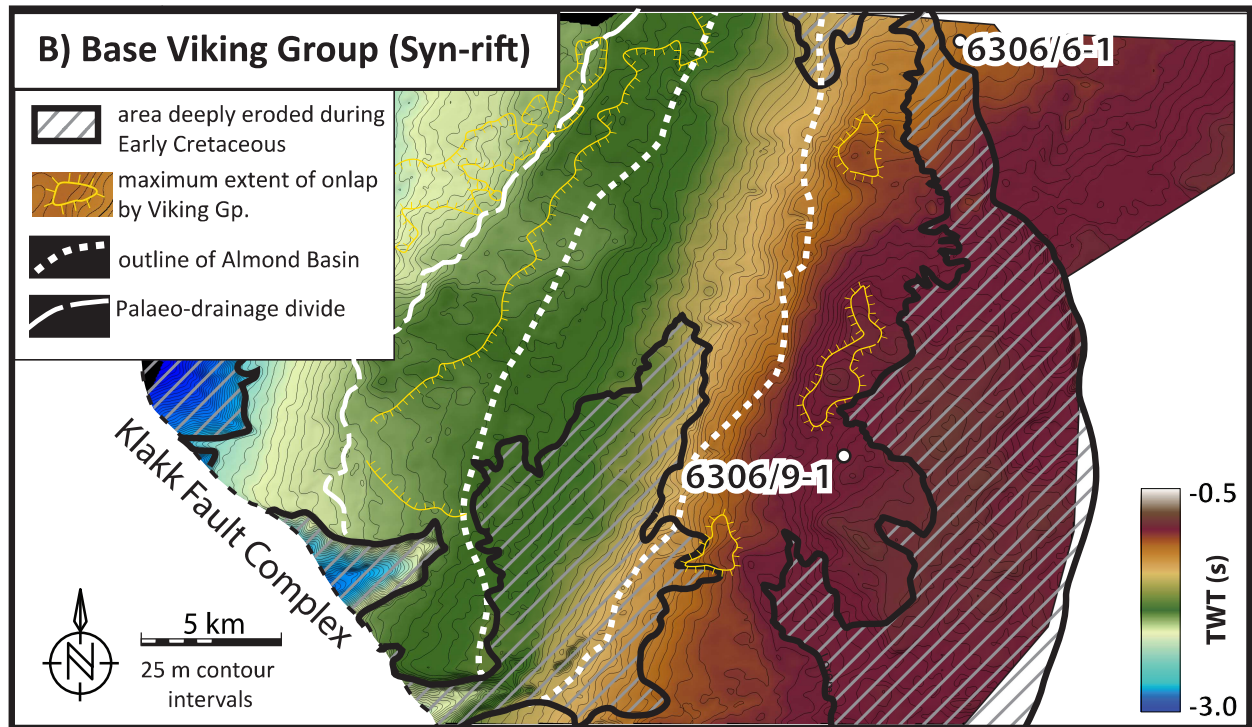
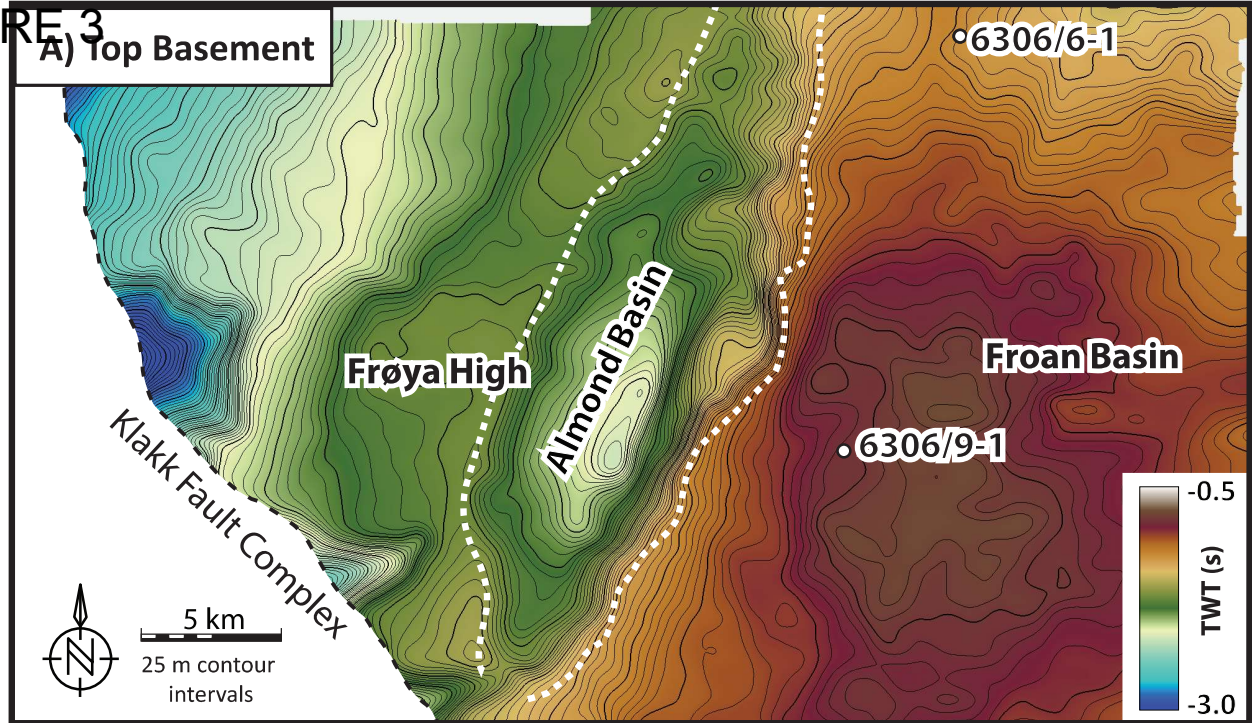


FIGURE 4

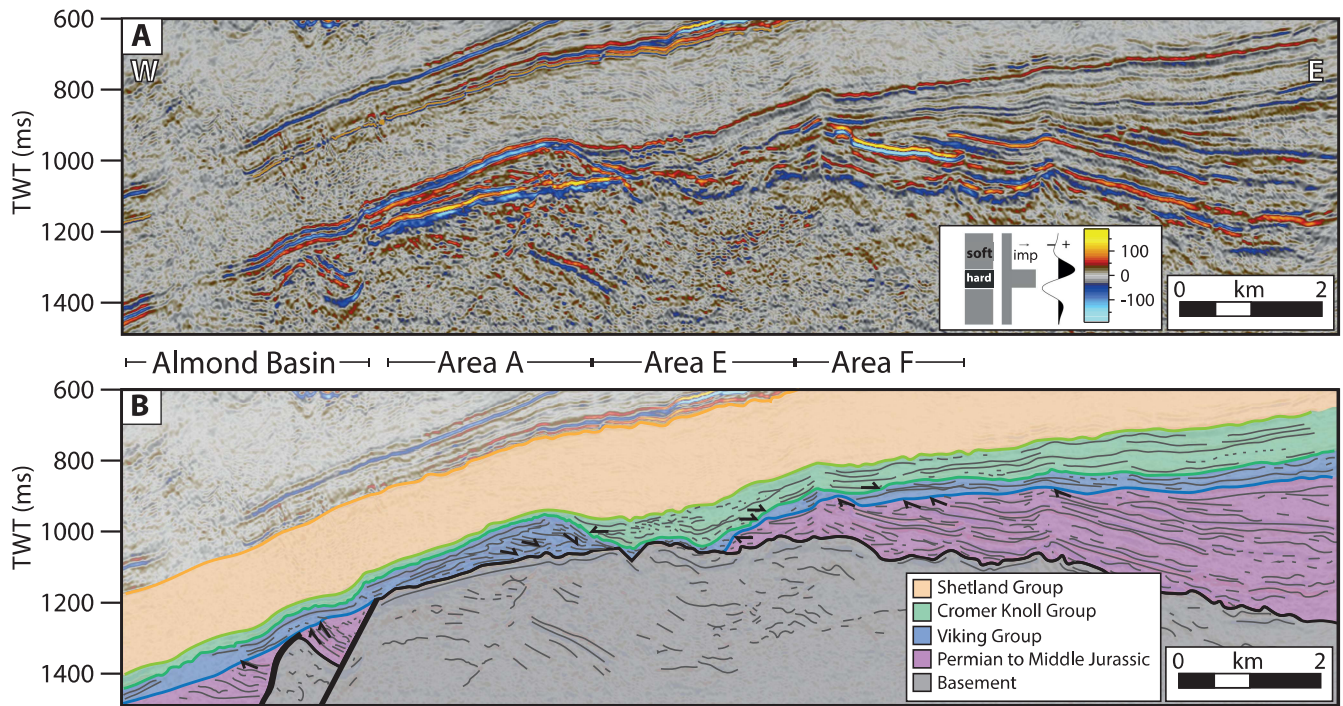
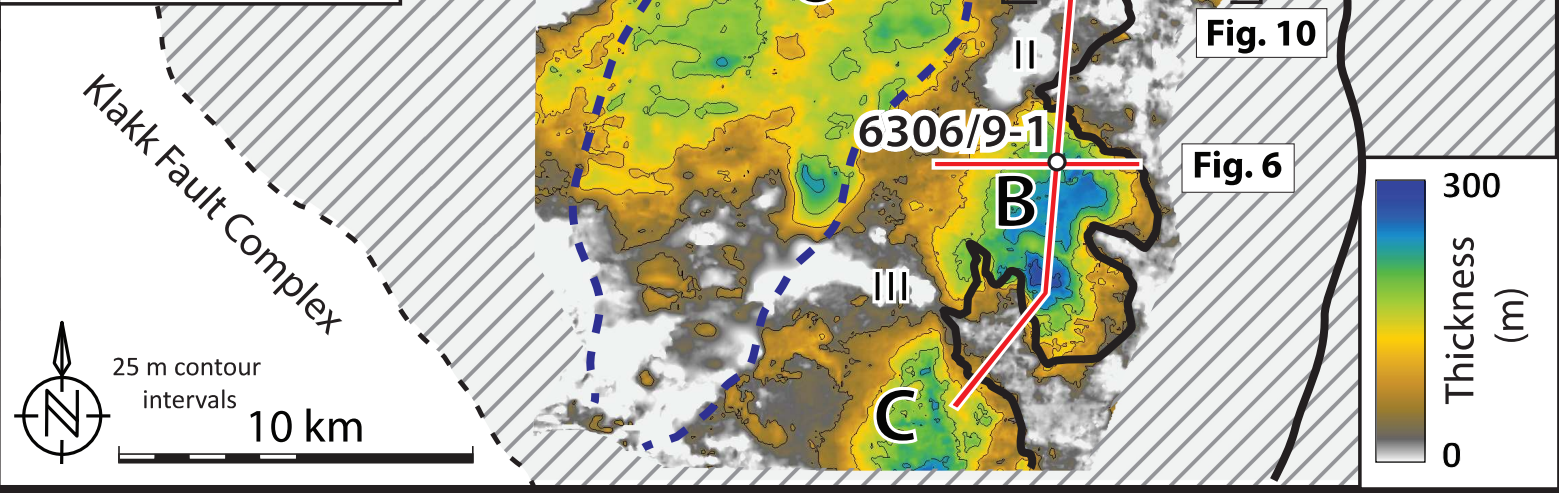


FIGURE 5

A) Syn-Rift Thickness (Viking Group)

- - - Almond Basin
- Trimmed from survey on Frøya High
- Heavily eroded region



B) Lower Post-Rift Thickness (Cromer Knoll Group)

- - - Almond Basin
- Trimmed from survey on Frøya High
- Heavily eroded region

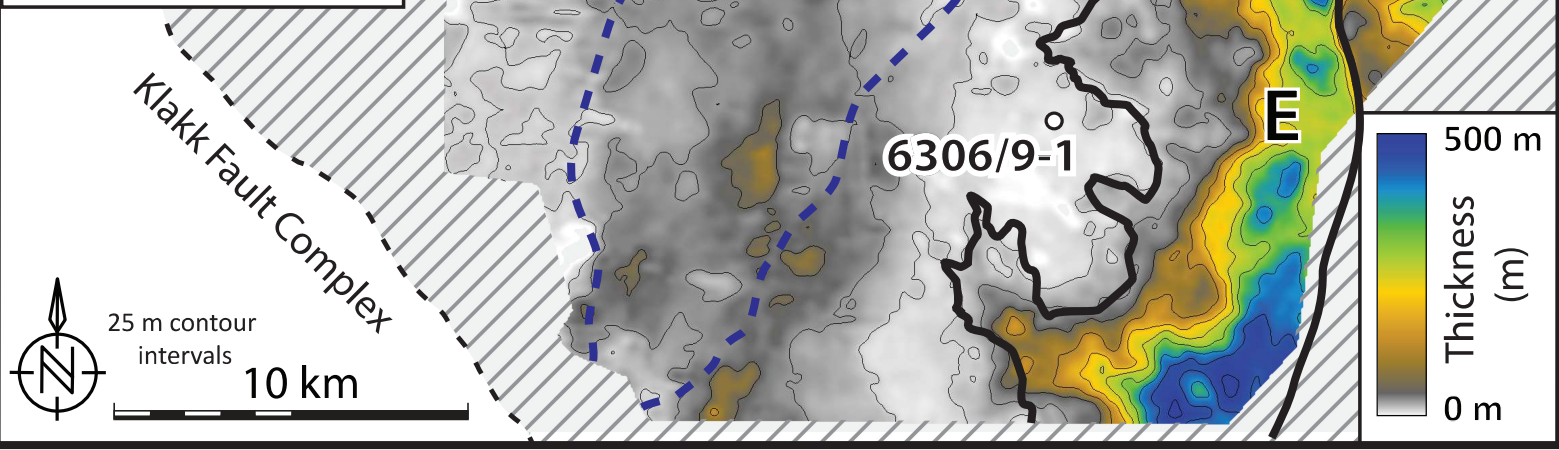


FIGURE 6

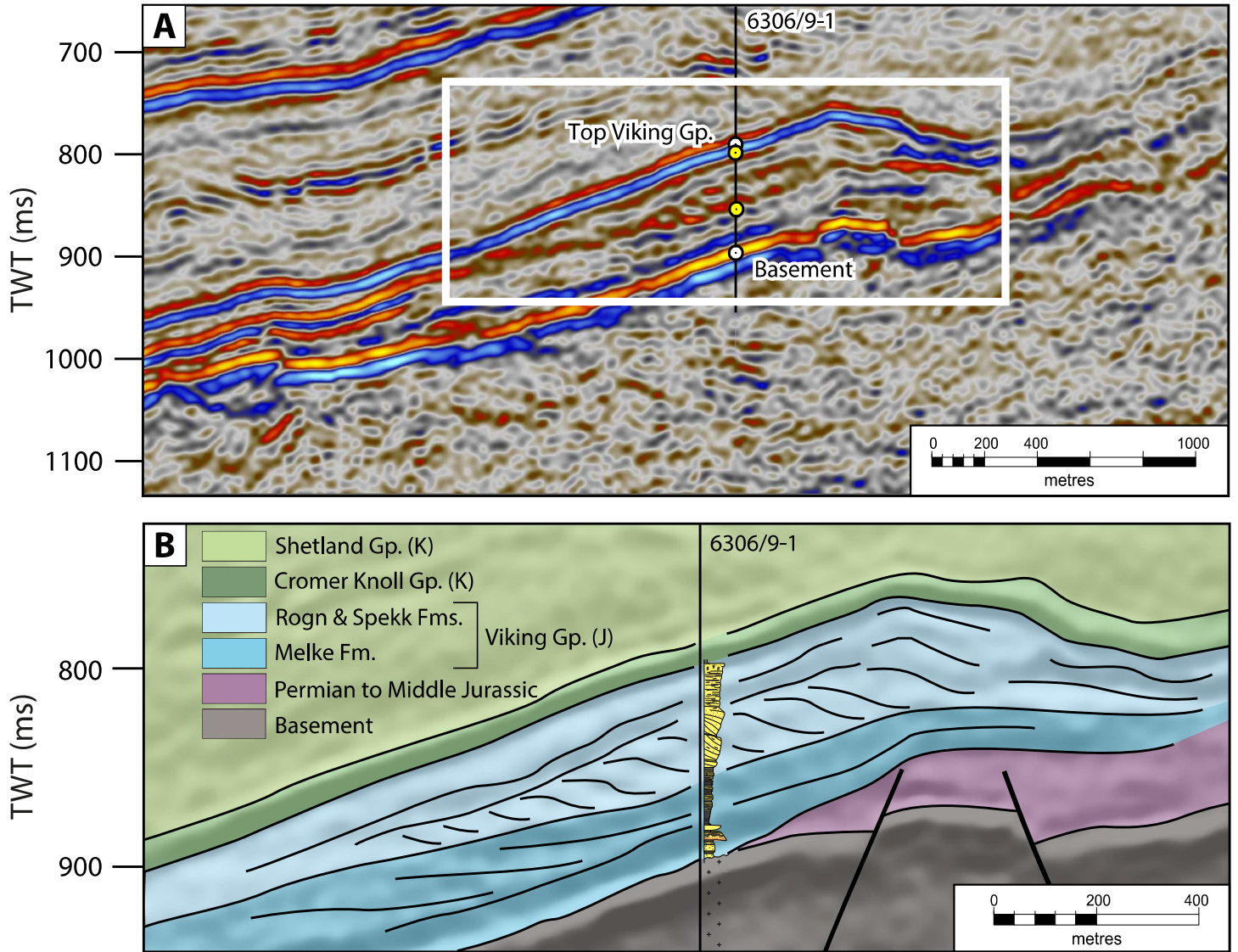


FIGURE 7

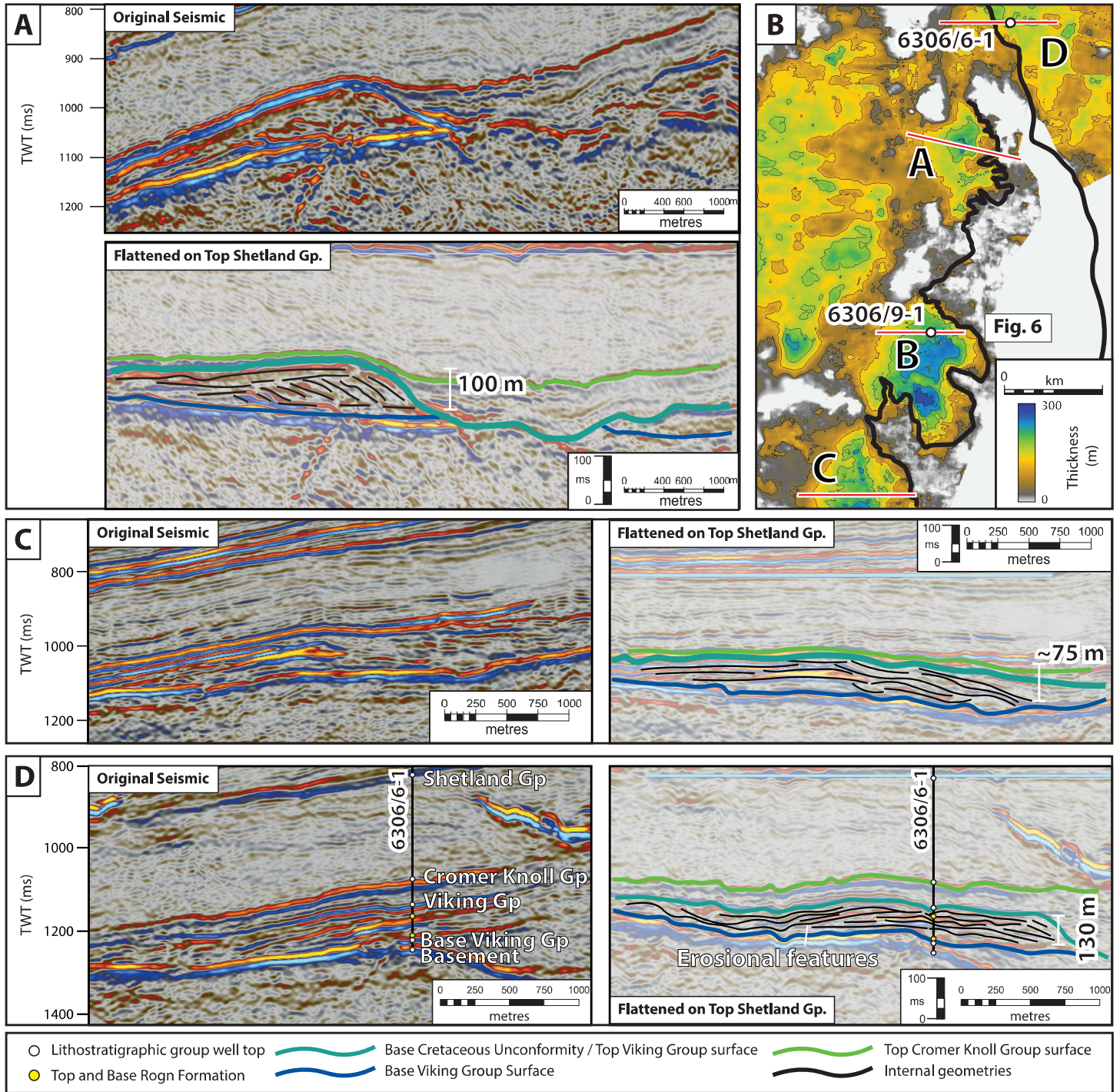


FIGURE 8

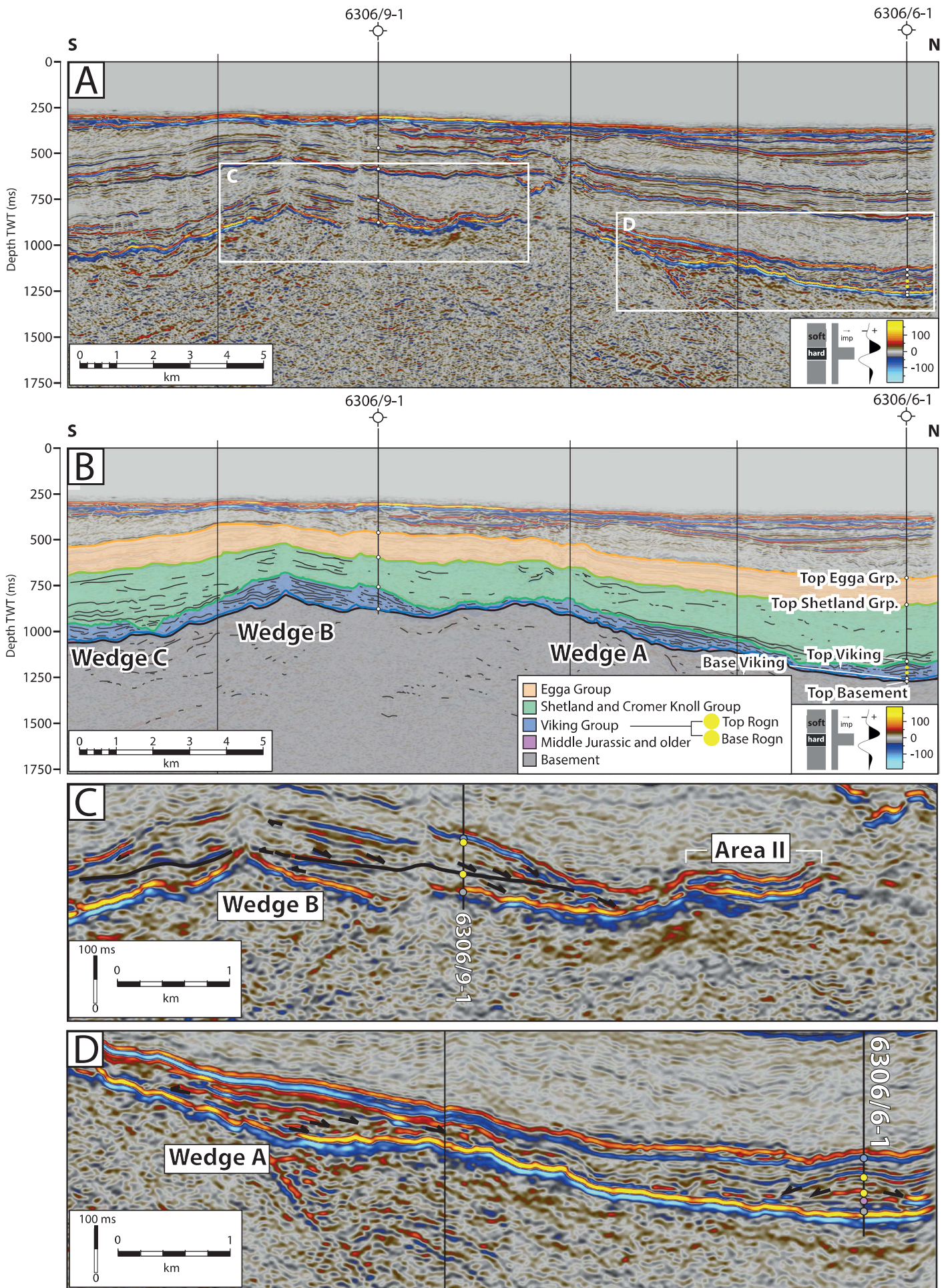


FIGURE 9

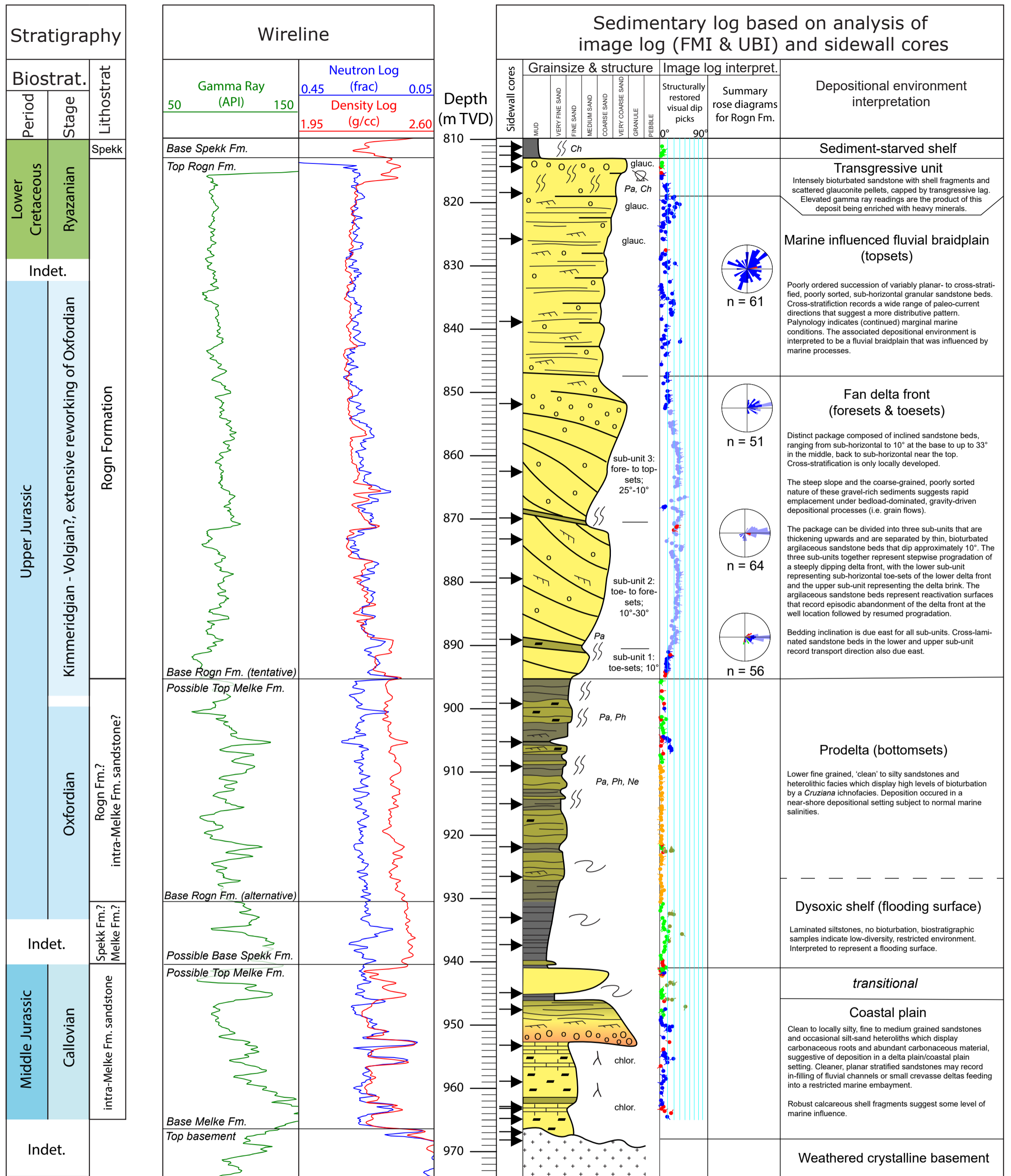


Image log interpretation 'tadpoles'	Ichonology	Sedimentology	Lithology
<ul style="list-style-type: none"> red dot: bed boundary green line: lamination (mudstone) orange line: lamination (heterolithic) blue line: lamination (sandstone) purple line: inclined bedding (sandstone) orange circle: conglomerate green circle: deformed bedding 	<ul style="list-style-type: none"> Ch: Chondrites Pa: Palaeophycus Ph: Phycosiphon Ne: Nereites 	<ul style="list-style-type: none"> - Organic fragments λ Root traces ∩ Intense burrowing — Cross-lamination o o Granules, pebbles ⊗ Shell fragments ~ Deformed bedding — Calcite cement glauc. Glauconitic pellets chlor. Chloritic pellets 	<ul style="list-style-type: none"> orange: conglomerate yellow: sandstone green: argillaceous sandstone grey: heterolithic black: mudstone

FIGURE 10

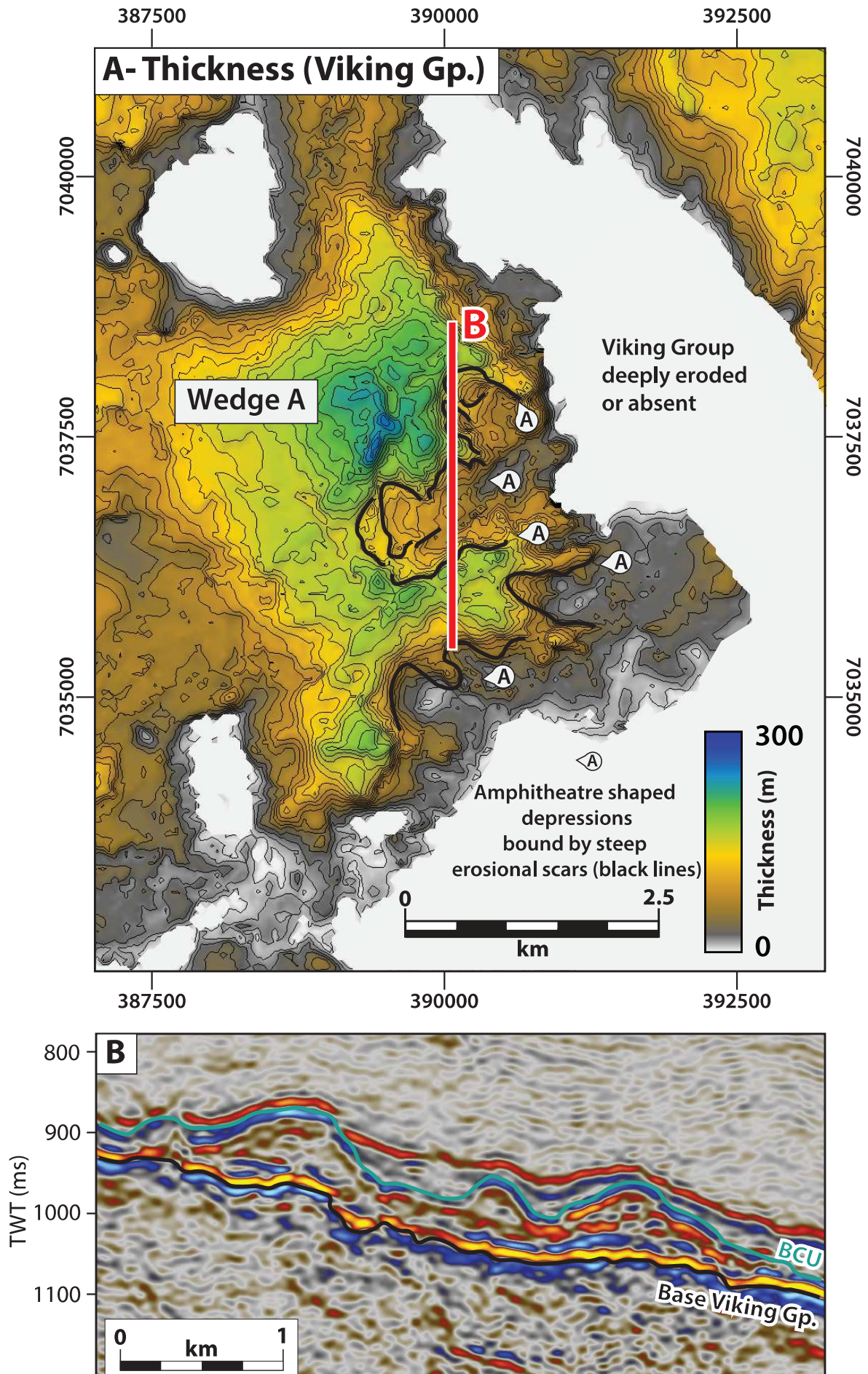
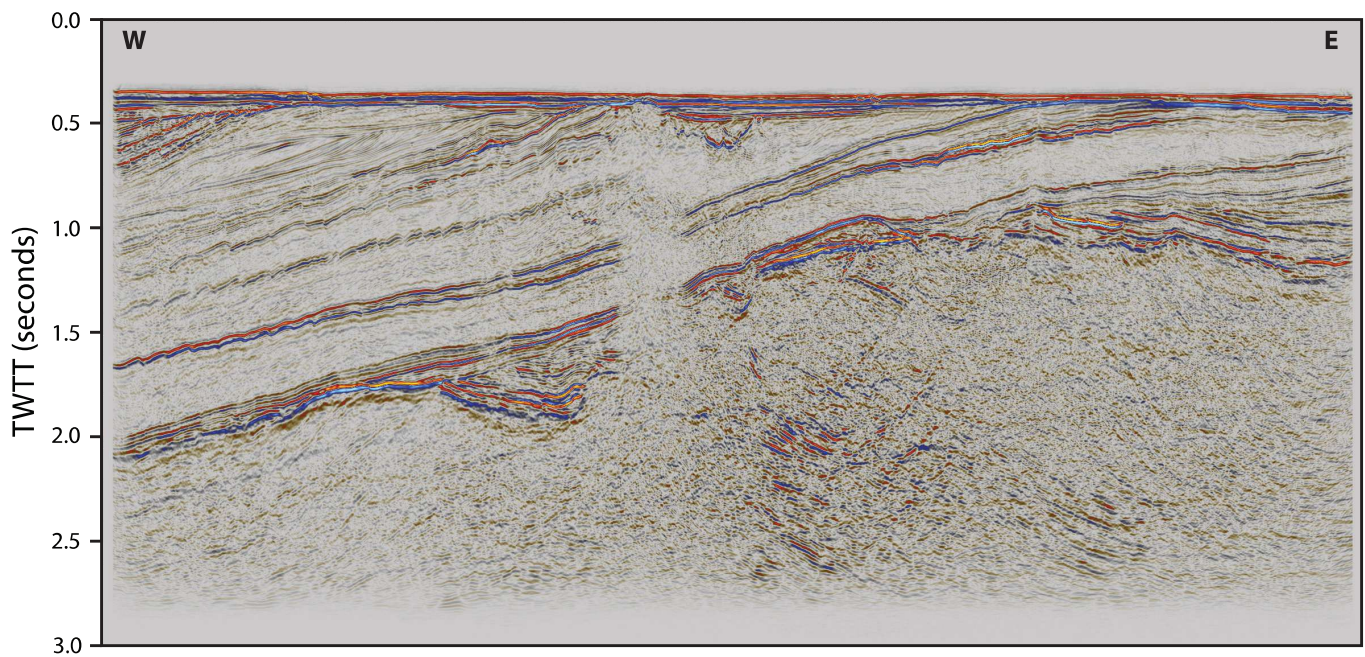
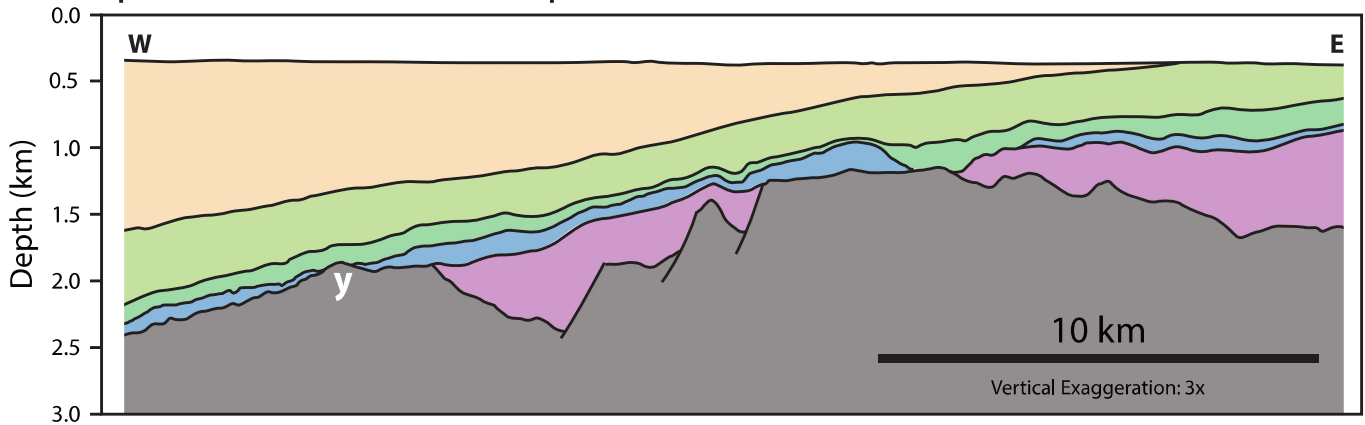


FIGURE 11

a) Seismic section



b) Depth-converted and interpreted section



c) Depth-converted and rotated section

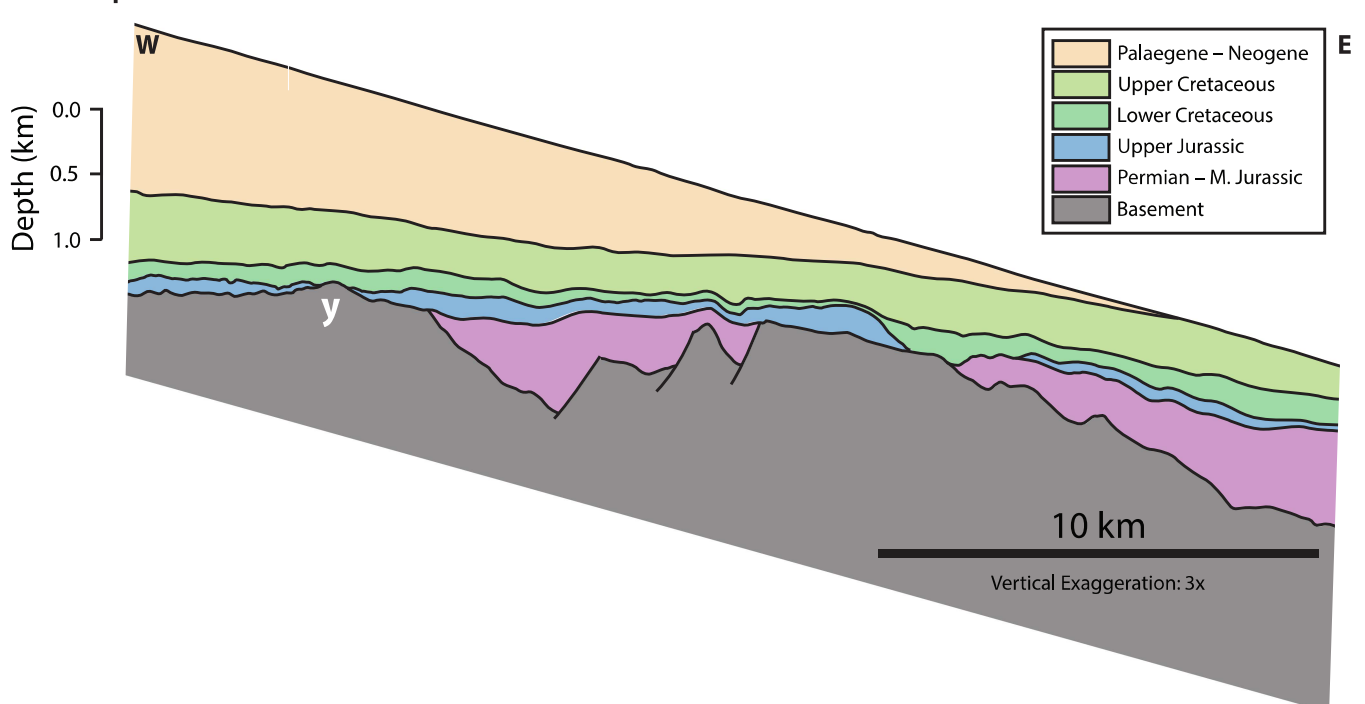


FIGURE 12

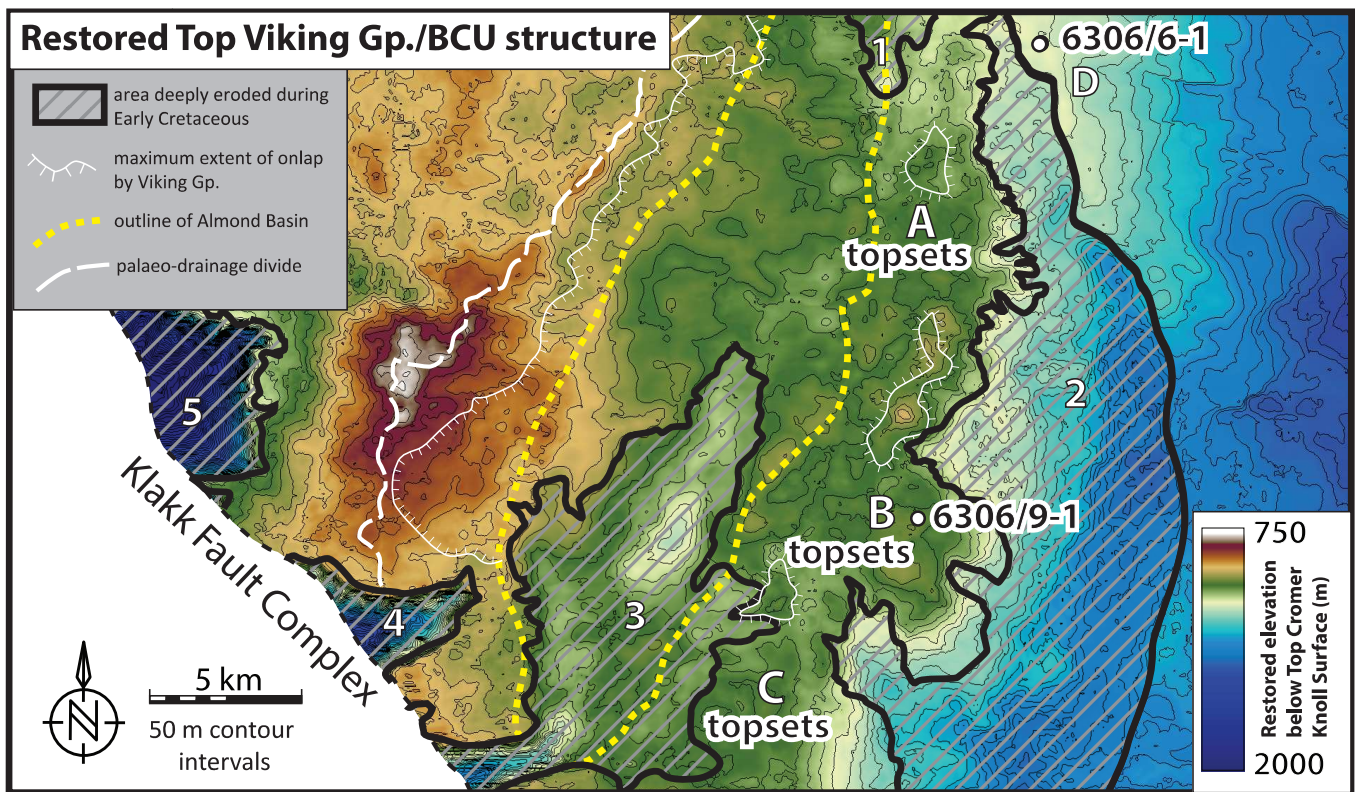
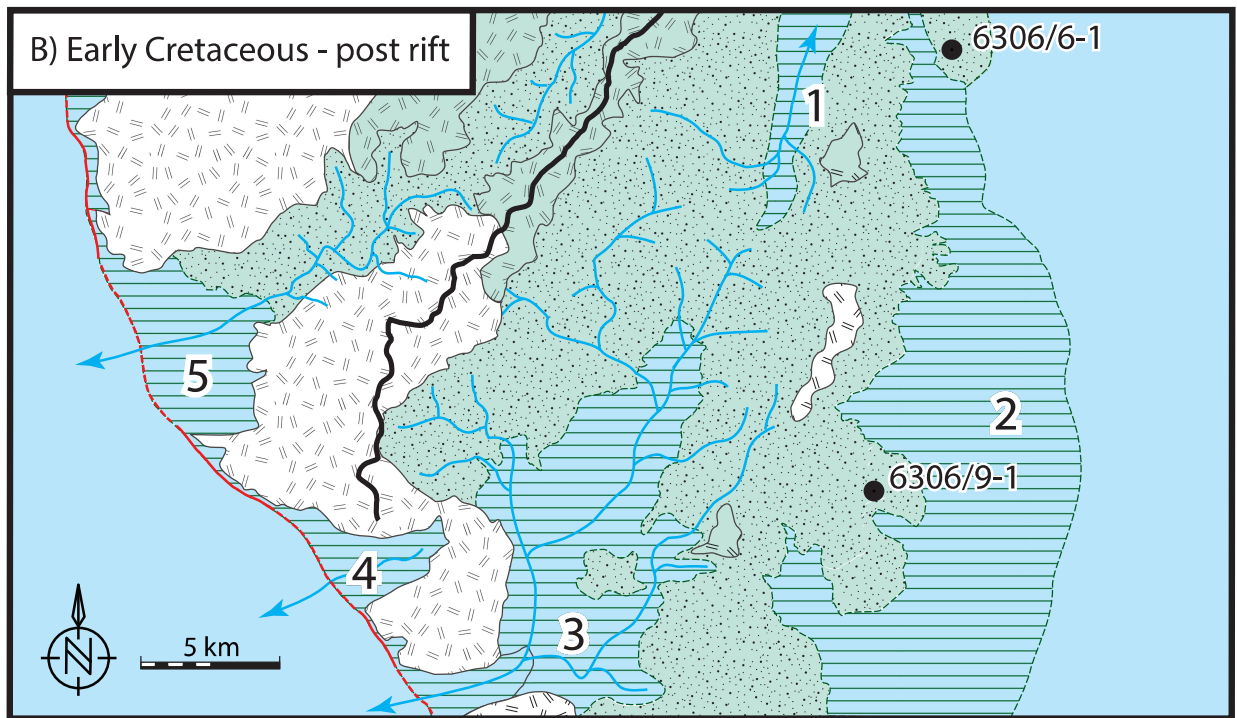
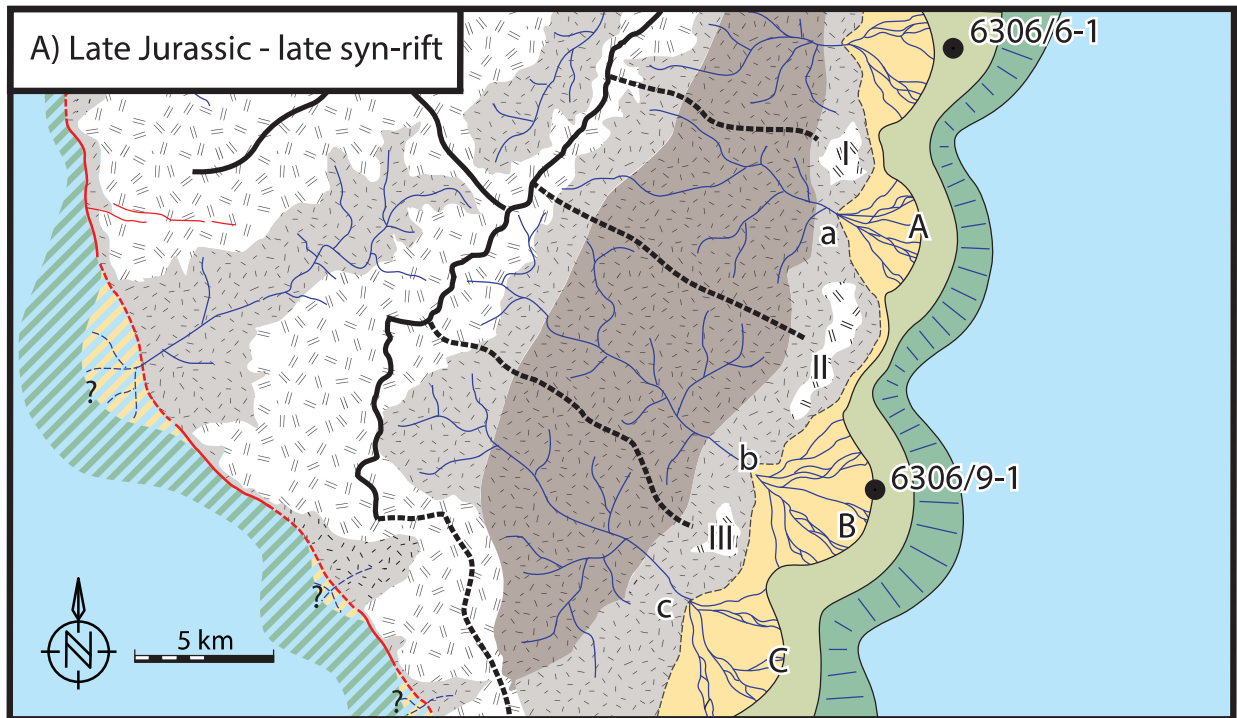


FIGURE 13



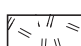
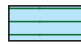

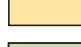









- | | |
|---|---|
|  Exposed crystalline basement |  Cretaceous canyon system |
|  Crystalline basement subcrop |  Subaerial delta plain |
|  Triassic-Lower Jurassic rocks subcropping the Upper Jurassic (The Almond Basin) |  Delta front platform |
|  Crystalline basement subcrop |  Delta front slope - prodelta |
|  Upper Jurassic subcrop |  Offshore |
| |  Drainage divide (estimated) |
| |  Drainage |
| |  Klakk Fault Complex |

Figure 14

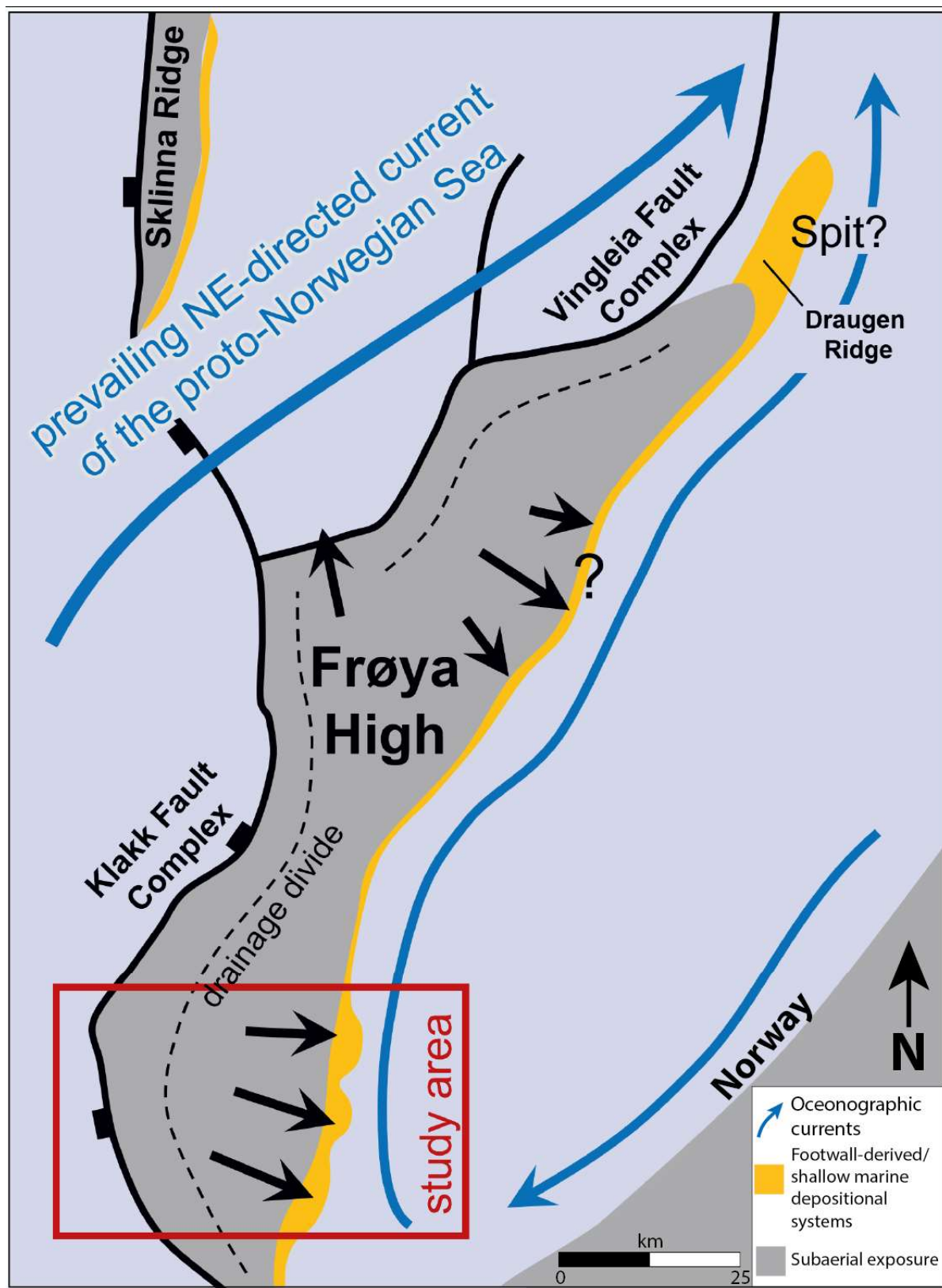


FIGURE 15

